 © 2012 Uspekhi Fizicheskikh Nauk, Russian Academy of Sciences

PHYSICS OF OUR DAYS

PACS numbers: **95.75.–z**, 98.70.Vc, **98.80.–k**

Searching for non-Gaussianity in observational cosmic microwave background data

O V Verkhodanov

DOI: 10.3367/UFNe.0182.201211d.1177

Contents

Abstract. **Methods for searching for non-Gaussianity in the WMAP data are reviewed and the associated problems related to the cosmic microwave background (CMB) data analysis are discussed. Evidence for non-Gaussianity has been obtained by various methods and from a number of multipole ranges. Different approaches to searching for non-Gaussian CMB data are sensitive to different manifestations of non-Gaussianity, which sometimes are due to the primordial non-Gaussianity and sometimes to galactic foregrounds and/or systematic residuals remaining after the data analysis that are difficult to take into account.**

1. Introduction

In the standard cosmological scenario with the Big Bang and simple inflation [1–5], quantum fluctuations of the scalar field generate inhomogeneities in the distribution of visible and dark matter [6–10], which leads to fluctuations in the microwave background radiation of the Universe. Temperature and polarization fluctuations of the cosmic microwave background (CMB) are expected, and confirmed at a certain level of precision by observations, to be Gaussian random fields, statistically isotropic in space. Nevertheless, certain models predict small but quite noticeable deviations of the signal from the Gaussian statistic and/or statistical isotropy, which, in principle, may be due to a number of reasons. Within the inflation theory, a relatively strong non-Gaussianity arises in models involving complex inflation [11–16] (for example, when a nonlinear relation exists between classical fluctuations of the scalar field generated at the inflation stage and the observed field of matter density fluctuations) (also see Refs [17–22]), while statistical anisotropy may be caused by anisotropic expansion at the inflationary stage [23–30], related, for instance, to the presence of classical vector fields. Other sources of non-Gaussianity and of statistical anisotropy, interesting from the standpoint of cosmology, could be a nontrivial topology of space [31–35], topological defects [36–39], anisotropic expansion [40, 41], the primordial magnetic field [42–46], etc. Owing to the appearance of new complete-sphere data [47], the issue of searching for and explaining the non-Gaussian properties of the CMB has become especially important.

Although non-Gaussianity and statistical anisotropy are far from being identical concepts, they are quite close to each other from a cosmological standpoint. Below, in discussing possible deviations from the simple picture of Gaussian and statistically isotropic fluctuations, we for brevity speak of non-Gaussianity, even though a number of CMB properties, such as the coaxiality of multipoles (see Sections 3.3 and 6) ought to be discussed in terms of statistical anisotropy.

O V Verkhodanov Special Astrophysical Observatory,
Russian Academy of Sciences,
369167 Nizhnii Arkhyz, Zelenchukskii region, Karachaevo-Cherkesskaya Respublika, Russian Federation
E-mail: vo@sao.ru

Received 13 July 2011, revised 1 December 1011
Uspekhi Fizicheskikh Nauk **182** (11) 1177 – 1193 (2012)
DOI: 10.3367/UFNr.0182.201211d.1177
Translated by G Pontecorvo; edited by A M Semikhatov

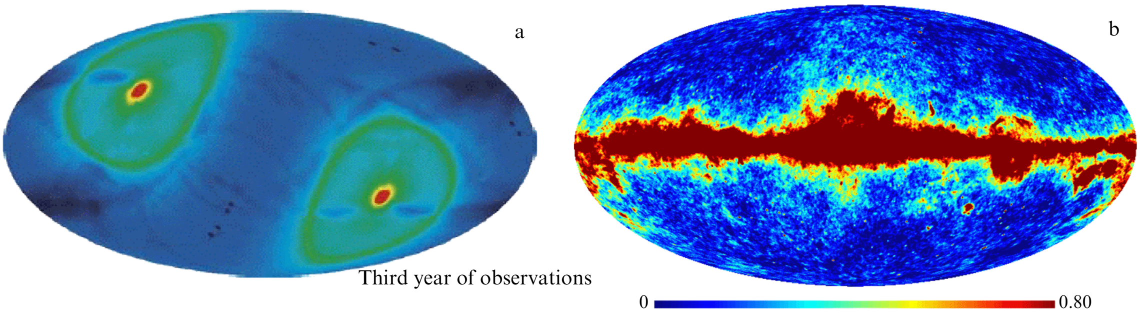

Figure 1. (See in color online.) (a) Example of a non-Gaussian effect due to the ecliptic coordinate system, manifested in sensitivity maps of the Wilkinson Microwave Anisotropy Probe (WMAP). (b) Example of a non-Gaussian effect due to the galactic coordinate system, related to galactic emission arriving mainly from the galactic plane; shown is the map of synchrotron radiation in the K-channel of WMAP.

Reliable establishment of the non-Gaussianity caused by processes that occurred in the early Universe would be of utmost importance for cosmology. Different cosmological scenarios lead to different forms of non-Gaussianity in density perturbations (see, e.g., Refs [48–58] and the references therein). For example, three-point and higher correlation functions exhibit extremely diverse dependences on coordinates or wave vectors. Therefore, the investigation of non-Gaussianity may help identify viable cosmological models. The investigation of CMB fluctuations is justified in being considered the most effective way of searching for non-Gaussianity [59]. The diversity of possible non-Gaussianity forms, however, also has a flip side: it is not known *a priori* which signal is to be sought and in which CMB characteristics the non-Gaussianity is manifested most strongly. The issue is also complicated by the fact that the CMB non-Gaussianity can be caused by effects related to the more recent Universe, such as CMB lensing [60, 61] and unaccounted pointlike sources.

There are also two more reasons giving rise to non-Gaussianity in the real signal appearing in CMB studies. They consist of the collection of systematic errors due to observational effects and/or effects caused by data handling (a non-Gaussian shape of the antenna pattern, peculiarities of microwave background observations in the ecliptic plane, and so on), and to the instability of algorithms used for separating signal components, which leads to residual contamination by galactic background components (Fig. 1), which are not well studied at small angular scales [62].

For searching for and analyzing the non-Gaussian properties of the CMB temperature, methods have been developed that use the distribution of temperature fluctuations over the celestial sphere, $\Delta T(\theta,\phi)$, where θ and ϕ are the angles in a polar coordinate system, as well as methods based on the expansion of temperature fluctuations with respect to spherical harmonics,

$$\Delta T(\theta,\phi)=\sum_{\ell=2}^{\infty}\sum_{m=-\ell}^{m=\ell} a_{\ell m}\,Y_{\ell m}(\theta,\phi)\,, \tag{1}$$

where $a_{\ell m}$ are complex quantities with the property

$$a^*_{\ell m}=a_{\ell,-m}\,, \tag{2}$$

which follows because temperature fluctuations $\Delta T(\theta,\phi)$ are real quantities. Theoretically, the relation between the primary inhomogeneities, representing adiabatic scalar perturbations, and the coefficients $a_{\ell m}$ is linear [63],

$$a_{\ell m}=(-\mathrm{i})^{\ell}\int\frac{\mathrm{d}^3\mathbf{k}}{(2\pi)^3}\,\Phi(\mathbf{k})\,g_{T\ell}(k)\,Y^*_{\ell m}(\hat{\mathbf{k}})\,, \tag{3}$$

where $\Phi(\mathbf{k})$ describes the primary perturbation of the density (more precisely, of the gravitational potential) in Fourier space, $g_{T\ell}(k)$ is the transfer function, and $\hat{\mathbf{k}}$ is the unity vector directed along the wave vector $\mathbf{k}$. A linear relation also exists between the temperature fluctuations $\Delta T(\theta,\phi)$ and the primary fluctuations $\Phi(\mathbf{k})$. The total radiation transfer function $g_{T\ell}(k)$ can be computed with the aid of the CMBFAST program [64]. A simple linear relation permits, at least theoretically, relating the CMB signal statistics and the statistics of primary perturbations: if the primary fluctuations $\Phi(\mathbf{k})$ are non-Gaussian, the non-Gaussianity can also be observed in the CMB. In sensitive surveys of the entire sky, for instance, the WMAP [1] and Planck [2] missions, it is already possible to search for deviations of the signal from the Gaussian statistics. We stress that expression (3) holds not only for adiabatic primary perturbations but also for constant-curvature modes [63] (with their own transfer functions).

We note an issue that must be raised in discussing the problems of CMB non-Gaussianity, related to the calculation of the angular power spectrum $C(\ell)$. By definition,

$$C(\ell)=\frac{1}{2\ell+1}\left(|a_{\ell 0}|^2+2\sum_{m=1}^{\ell}|a_{\ell m}|^2\right), \tag{4}$$

and the coefficients $a_{\ell m}$ are obtained by transforming the map into harmonics:

$$a_{\ell m}=\int_0^{\pi}\sin\theta\,\mathrm{d}\theta\int_0^{2\pi}\mathrm{d}\phi\,\Delta T(x,\phi)\,Y^*_{\ell m}(x,\phi)\,. \tag{5}$$

In expression (4), a Gaussian distribution is implied for the $2\ell+1$ coefficients $a_{\ell m}$, whose squared amplitudes are averaged with the same weights. In this case, the two-point correlator (with the averaging performed over the ensemble of universes) has the form

$$\langle a_{\ell m}a^*_{\ell' m'}\rangle=C_\ell\,\delta_{\ell\ell'}\delta_{mm'}\,. \tag{6}$$

[1] http://lambda.gsfc.nasa.gov
[2] http://www.rssd.esa.int/Planck/

In the case of averaging at a given ℓ, the meaning of the quantity C_ℓ for non-Gaussian data is no longer obvious.

The simplest and best studied quantity in which the non-Gaussianity of CMB fluctuations may be manifested is the three-point correlation function or its harmonic analog, the bispectrum

$$\langle a_{\ell_1 m_1} a_{\ell_2 m_2} a_{\ell_3 m_3} \rangle \,. \tag{7}$$

The bispectrum is quite sensitive to certain forms of non-Guassianity that are considered 'standard'. These include the so-called local form obtained under the assumption that primary fluctuations exhibit a nonlinearity local in the coordinate space [63]:

$$\Phi(x) = \Phi_{\mathrm{L}}(x) + f_{\mathrm{NL}}\left(\Phi_{\mathrm{L}}^2(x) - \left\langle \Phi_{\mathrm{L}}^2(x) \right\rangle\right), \tag{8}$$

where $\Phi_{\mathrm{L}}(x)$ denotes a linear Gaussian field, $\langle \Phi_{\mathrm{L}}(x) \rangle = 0$, and f_{NL} is a constant describing the nonlinearity in the form of a quadratic correction to perturbations of the gravitational potential (curvature). Such a form of non-Gaussianity indeed arises in some inflationary models involving an additional scalar field (curvaton) [12, 65, 66] and/or the nontrivial dynamics of postinflational modulated heating [14, 15]. The 'equilateral' [67] and 'orthogonal' [68] forms of non-Gaussianity are also considered to be 'standard'. The WMAP mission team devoted some of its work [22, 69–72] to the investigation of these and of certain other forms of non-Gaussianity, the main instrument being precisely the angular bispectrum of the CMB temperature. The authors of Ref. [72] established the results of an analysis of seven-year-long observations performed by the WMAP mission to be consistent, at a 95% confidence level, with the hypothesis that primary fluctuations are Gaussian, and upon combining their results with those of the Sloan Digital Sky Survey (SDSS) ($-29 < f_{\mathrm{NL}} < 70$ [73]) they found, in particular, that $-5 < f_{\mathrm{NL}} < 59$.

Various methods are used in studying peculiarities of the radiation distribution over the celestial sphere, depending on statistical properties of the CMB signal investigated, on the resolution parameter ℓ describing angular scales on the sphere, and on the specific goals to be achieved. During the years that have passed since the WMAP mission data became available [69, 74–79], announcements have been made concerning a number of deviations from non-Gaussianity and statistical isotropy [80–98] exhibited by the distribution of the CMB signal. Several tests based on phase analysis, multipole vectors, Minkowski functionals, wavelets and needlets, the bispectrum and trispectrum, etc., have been proposed for verification and investigation of the non-Gaussianity. In this article, we examine some of these methods (applied in the aforementioned references in dealing with data from the WMAP mission), whose main advantage consists in the repeated, multi-frequency complete coverage of the sky. Precisely this fact has made extensive application of the methods described in this article possible. It must be noted that observations of the CMB radiation performed by the WMAP mission of NASA and their further presentation to the astronomical community in the archive of WMAP observations turned out to be a revolutionary step in modern cosmology.

To conclude this section, we note that no definite answer to the question concerning the presence or absence of non-Gaussian features in the statistics of primary density perturbations has yet been obtained. Certain peculiarities to be discussed in this article could perfectly well be caused by the aforementioned systematic effects and the instability of the algorithms used for separating the components; others may simply be statistical fluctuations. In the latter case, as underlined by the WMAP team [69], estimations of the statistical significance of anomalies are made difficult by their having been observed a posteriori and often involving parameters whose values were chosen on purpose to achieve a non-Gaussian signal as large as possible.

2. The CMB map

Besides CMB, the signal measured in experiments involves contributions from galactic background components and from galactic and extragalactic radio sources. These can be taken into account by superposing masks, i.e., by excluding certain patches of the celestial sphere from consideration (22% in the case of the KQ85y7 mask used for the data collected over seven years by the WMAP mission [99]). It is possible, however, to restore the CMB signal over the whole celestial sphere using the results of the WMAP multifrequency observations. One of the methods for determining the complete CMB temperature map is based on a combination of observational data at different frequencies, additionally multiplied by certain coefficients permitting the exclusion of the galactic signal from the result and, thus, singling out the microwave relic background [77]. In this approach, the idea is used that the radiation spectra of galactic background components (namely, of synchrotron radiation, free–free radiation, and of the radiation of dust) differ from the CMB spectrum. Because the combination of channels in the WMAP mission is achieved without using observations from other experiments, this method has been termed Internal Linear Combination (ILC). The coefficients can be determined by minimizing the dispersion in the resultant map, equating their sum to unity, so as to preserve the overall normalization of the CMB signal.

In describing this procedure, we first note that from the results of simulation [77], the instrumental noise has been established to not affect the situation significantly, because it only provides a shift of the order of 10 μK in the estimate of the signal in the galactic plane. In the simple case where the instrumental noise can be neglected and the background components have the same spectrum in the region investigated and differ from each other in different parts of this region only in temperature, the sought ILC temperature can be written as a linear combination of signals from the maps for different frequencies ν_i:

$$\begin{aligned} T_{\mathrm{ILC}}(p) &= \sum_i \zeta_i T_i(p) = \sum_i \zeta_i \left[T_{\mathrm{c}}(p) + S_i T_{\mathrm{f}}(p)\right] \\ &= T_{\mathrm{c}}(p) + \Gamma T_{\mathrm{f}}(p)\,. \end{aligned} \tag{9}$$

Here, $T_i(p) \equiv T(\nu_i, p)$ is the map of the signal observed at the frequency ν_i, p is a certain pixel of the image (the smallest region of the map with the measured temperature), the map of the signal $T_i(p) = T_{\mathrm{c}}(p) + S_i T_{\mathrm{f}}(p)$ is represented as a sum of the CMB maps $T_{\mathrm{c}}(p)$ and of the background component $S_i T_{\mathrm{f}}(p)$, the coefficient $S_i \equiv S(\nu_i)$ describes the total frequency spectrum of background radiation, and $T_{\mathrm{f}}(p)$ is the distribution of the background radiation temperature. The coefficients ζ_i that are to be determined satisfy the normalization condition $\sum_i \zeta_i = 1$. The notation $\Gamma \equiv \sum_i \zeta_i S_i$ is introduced in (9).

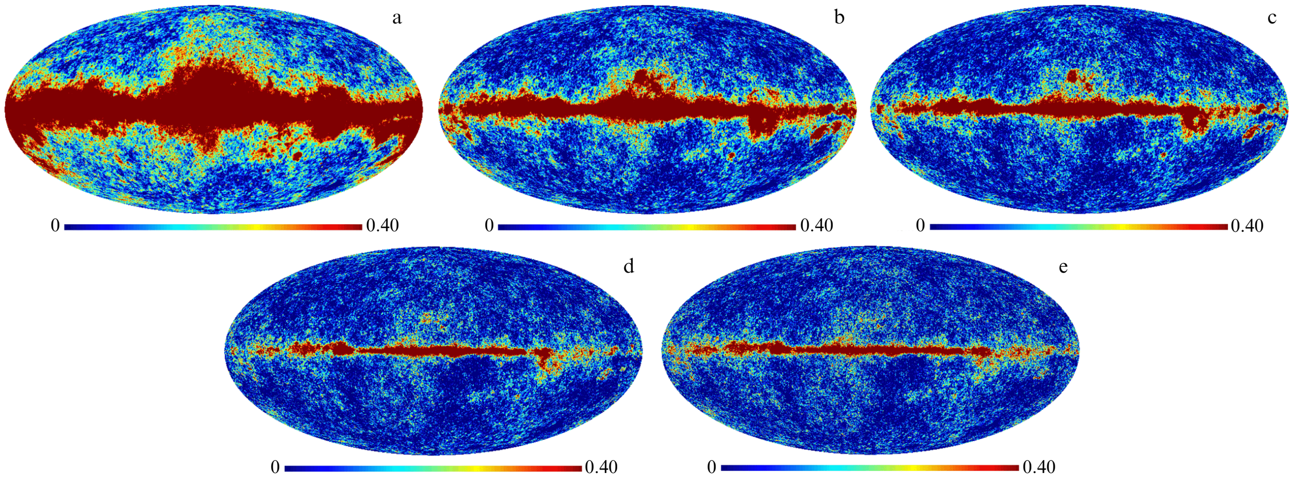

Figure 2. (See in color online.) Maps of the observed microwave radiation in WMAP frequency channels: (a) 23 GHz (band K), (b) 33 GHz (band Ka), (c) 41 GHz (band Q), (d) 61 GHz (band V), and (e) 94 GHz (band W) from data obtained during the seventh year of WMAP observations. The maps are produced in galactic coordinates.

The coefficients ζ_i are determined by minimizing the dispersion of $T_{\rm ILC}(p)$. For this dispersion, we have [77]

$$\sigma_{\rm ILC}^2 = \left\langle T_{\rm ILC}^2(p)\right\rangle - \left\langle T_{\rm ILC}(p)\right\rangle^2$$
$$= \langle T_{\rm c}^2\rangle - \langle T_{\rm c}\rangle^2 + 2\Gamma\left[\langle T_{\rm c}T_{\rm f}\rangle - \langle T_{\rm c}\rangle\langle T_{\rm f}\rangle\right]$$
$$+\,\Gamma^2\left[\langle T_{\rm f}^2\rangle - \langle T_{\rm f}\rangle^2\right] = \sigma_{\rm c}^2 + 2\Gamma\sigma_{\rm cf} + \Gamma^2\sigma_{\rm f}^2\,, \qquad (10)$$

where the angular brackets $\langle\ldots\rangle$ denote averaging over the pixels of the selected region. The minimization of $\sigma_{\rm ILC}^2$,

$$0 = \frac{\delta\sigma_{\rm ILC}^2}{\delta\zeta_i} = 2\,\frac{\delta\Gamma}{\delta\zeta_i}\,\sigma_{\rm cf} + 2\Gamma\,\frac{\delta\Gamma}{\delta\zeta_i}\,\sigma_f\,, \qquad (11)$$

yields $\Gamma = -\sigma_{\rm cf}/\sigma_{\rm f}^2$ and

$$T_{\rm ILC}(p) = T_{\rm c}(p) - \frac{\sigma_{\rm cf}}{\sigma_{\rm f}^2}\,T_{\rm f}(p)\,.$$

In the ideal case, where no correlation between the CMB and the background exists, i.e., $\sigma_{\rm cf} = 0$, the ILC map coincides with the CMB map. Actually, as emphasized in Ref. [77], the ILC map is shifted toward a decrease in the correlation between the CMB signal and the signal from background components.

We note that different versions of the ILC method exist in both pixel space and harmonic space (see the review in Ref. [100]). The regions where this method is used can be determined as follows: (1) by dividing the sphere into separate zones [77] (for example, in the analysis of WMAP data, the sphere was divided into 12 regions, most of which were situated in the galactic plane); (2) by applying selection rules for averaged pixels [101]; (3) by fixing a certain set of harmonics [102]. It is also possible to use other combinations of radio-frequency observations. The modifications result in only a few different maps being obtained. Moreover, there are different versions of the actual procedure for producing a map of an internal linear combination (for instance, the Lagrange ILC, LILC, method [86], which yields the same results as ILC). Finally, separation of the signal components and the production of CMB maps is also possible with other methods, such as the Maximum Entropy Method (MEM) [77, 103], fitting templates of background components to other observations [77, 103], Wiener filtration (the Wiener-filtered map, WFM) performed in [104], or weighted removal of the background (the foreground-cleaned map (FCM) in [104]). The last was used to produce CMB maps exhibiting a higher resolution ($\ell_{\max} = 600$) than the WMAP. In what follows, we mainly deal with the ILC WMAP map, although maps obtained by other methods are also mentioned.

Observations were performed by the WMAP within five frequency bands: 23 GHz (band K), 33 GHz (band Ka), 4 GHz (band Q), 61 GHz (band V), and 94 GHz (band W) (Fig. 2), involving intensity and polarization measurements. Data arrays collected by the mission during one, three, five, and seven years of work were put on a website for general use [74–79]. As a result of observational data processing, which included the registration and storage of time series, map making and sky pixelization, and the separation of signal components and their subsequent analysis, data were obtained on the anisotropy and polarization distributions of the CMB and of background components (synchrotron and free–free radiation, the radiation of dust), and their power spectra were also calculated. The ILC WMAP map produced was smoothed out by a Gaussian-shaped diagram with a 1° resolution. The entire archive of observational and processed data is available and accessible to the scientific community at the WMAP website.

In Fig. 3, a map of the CMB anisotropy distribution reconstructed by the ILC method is presented for not very high harmonics ($\ell \leqslant 150$). Figure 4 shows the angular power spectrum produced using data from the WMAP mission and from the ACBAR (Arcminute Cosmology Bolometer Array Receiver) [105] and QUaD (QUEST (Q and U Extragalactic Sub-mm Telescope) at DASI) experiments [106].

3. Phase analysis

The discovery of non-Gaussian properties in WMAP data was first announced in publications [74–76] on the investigation of the statistics obtained by the mission during its first year of work by methods of the phase analysis of signals [80–82]. Although after presenting the CMB maps, the WMAP team declared the identified signal to be Gaussian at a

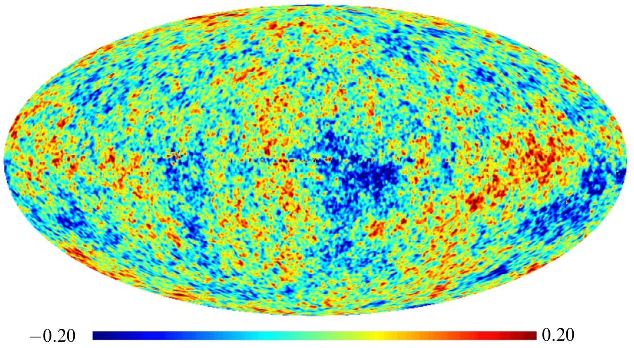

Figure 3. (See in color online.) The ILC CMB map made in galactic coordinates and based on the data obtained by the WMAP during its seventh year of work (shown with a resolution of up to $\ell_{\max} = 150$).

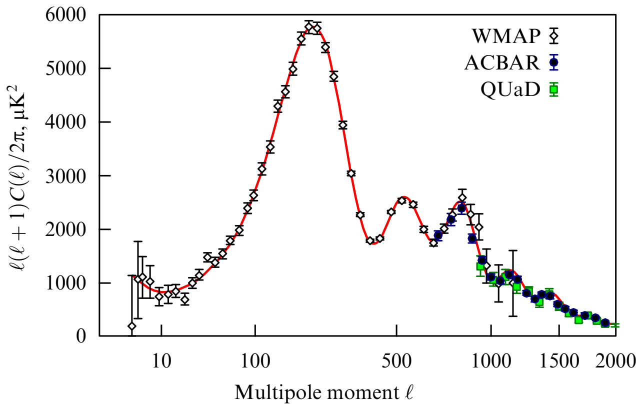

Figure 4. (See in color online.) Angular power spectrum $\ell(\ell+1)C(\ell)/(2\pi)$ of a WMAP map for the seventh year of observations [72] and measurement results of the angular power spectrum of temperature fluctuations in the ACBAR [105] and QUaD [106] experiments. The results are shown for the multipole region up to $\ell < 2000$, within which the contribution of the Zel'dovich–Sunyaev effect and of point sources is not too high. The solid curve shows the simulated spectrum for Lambda Cold Dark Matter (ΛCDM) cosmology with parameters determined on the basis of WMAP results.

confidence level of 95% [76], the ILC map was also noted to exhibit 'complex noise properties'.[3]

Phase analysis of a signal is based on the fact that the multipole coefficients $a_{\ell m}$ present in formula (1) are complex and that they can be represented as

$$a_{\ell m} = |a_{\ell m}| \exp(\mathrm{i}\phi_{\ell m}) \,, \tag{12}$$

where $\phi_{\ell m}$ is the phase of the (ℓ, m) harmonic. It follows from (2) that for $m = 0$ and all ℓ, $\phi_{\ell,0} = 0$, and $\phi_{\ell,-m} = -\phi_{\ell m}$. The Fourier modes of homogeneous and isotropic Gaussian fields have real and complex parts whose distributions are independent of each other. Therefore, if the primary inhomogeneities of density represent a homogeneous and isotropic field in space, they lead to phases $\phi_{\ell m}$ that are independently and homogeneously distributed within the interval $[0, 2\pi]$ [107, 108], which is precisely consistent with relation (6).

The rigorous definition of a homogeneous and isotropic Gaussian random field requires the amplitude to be Rayleigh distributed and the phase to be randomly distributed [109]. At the same time, the central limit theorem guarantees that the superposition of a large number of random-phase Fourier modes is Gaussian. Therefore, the requirement that the distribution of phases be random and homogeneous actually serves in and of itself as the definition of Gaussianity [107]. If the data analyzed are non-Gaussian, then, as has been mentioned, this may signify that either certain mechanisms in the early Universe gave rise to non-Gaussian density inhomogeneities or that there are systematic effects not taken into account.

[3] http://lambda.gsfc.nasa.gov/product/map/m_products.html

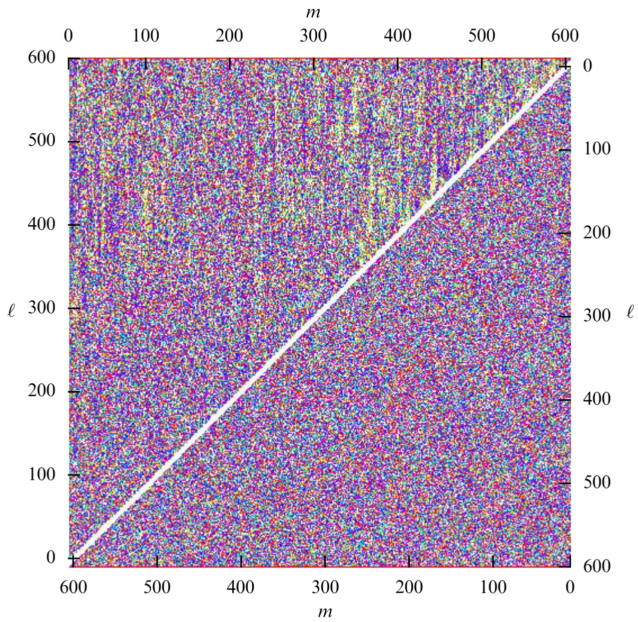

Figure 5. (See in color online.) Color phase diagram of the gradient D_ℓ for the FCM (upper left triangle) and WFM (lower right triangle) maps. 256 colors reproduce the phase intervals within the $[0, 2\pi]$ interval for which phases are taken from the complex representation of harmonics. The vertical axis shows the multipole numbers ℓ and the horizontal axis shows the multipole modes m, $m \leqslant \ell$. Owing to the relation $a_{\ell,m} = a^*_{\ell,-m}$, only modes with nonnegative m are presented. (See Ref. [80] for the details.)

3.1 Colored phase diagrams and non-Gaussianity at high multipoles ($100 < \ell \leqslant 400$)

Coles and Chiang [110] were among the first authors who applied color visualization for the demonstration of phase relations. Without going into the details of visualization methods, we note that the most suitable for phase visualization is the hue–saturation–brightness (HSB) method. In this method, the primary colors — red, green, and blue — correspond to phases 0, 120°, and 240°, while the complementary colors (cyan, magenta, and yellow) respectively correspond to the intermediate phases 60°, 180°, and 300°. As the phase changes, the colors smoothly 'flow' into each other, magenta becoming red, which is consistent with phases 360° and 0° being identical.

The method of phase map making was applied in Ref. [80] to CMB data, with a high resolution achieved in [104]. Figure 5 shows the color encoding of the phase gradient $D_\ell \equiv \phi_{\ell+1,m} - \phi_{\ell,m}$ for the FCM and WFM maps in [104]. Although finding the phase gradient for neighboring modes is the most primitive way of testing phase correlations, the visible presence of bands in the FCM phase map points to a strong correlation between multipoles of identical modes m of multipoles with adjacent ℓ. At the same time, the phase

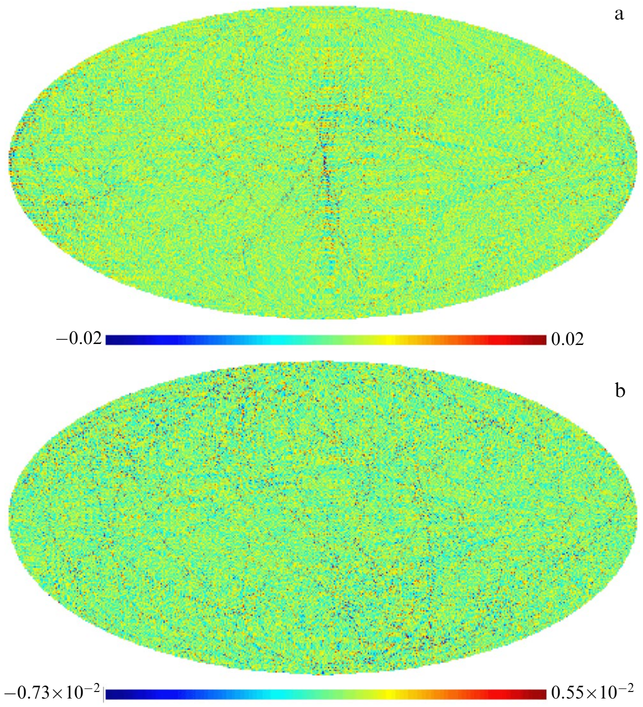

Figure 6. (See in color online.) Contribution to CMB temperature variations from two multipoles, $\ell = 350$ and 352, for (a) FCM and (b) WFM maps in galactic coordinates. The choice of multipoles is determined by the discovery of phase coupling for harmonics with $\Delta\ell = 2$ in the FCM map. The structure seen in the FCM map at $\varphi \simeq 0$ and π, which is perpendicular to the plane of the Galaxy and passes through its center, vanishes in the WFM maps obtained by Weiner filtration, making them practically Gaussian for these multipoles. (See the details in Ref. [80].)

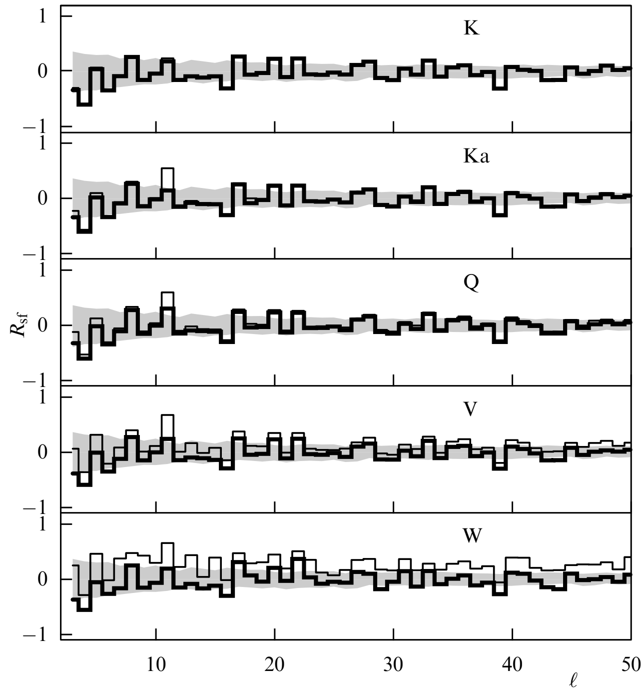

Figure 7. The circular correlation coefficient between the phases of the ILC CMB signal and of galactic components in the channels K – W versus the harmonic number ℓ. The thick line corresponds to the result of correlations with the phases of the background component, made available by the WMAP. The thin line corresponds to data of the background obtained from the difference between the general WMAP signal in the given channel and the ILC CMB signal. The shaded region shows the level of uncertainty 1σ, determined from the results of 200 random simulations. (See also Refs [81, 112].)

diagram for the WFM map shows a homogeneous distribution of phases consistent with the Gaussianity of the signal.

The authors of Ref. [80] checked the phase 'randomness' more rigorously, using simulations to obtain statistical estimates of phase deviations [80, 111]. For this, 2000 simulations of random Gaussian fields were performed, which resulted in the deviation from Gaussianity being revealed for several multipole ranges in the region of $\ell \simeq 150$, 290, 400, and 500 at a confidence level exceeding 95% [80]. An example of such harmonics, whose phases deviate significantly from those statistically expected ($\ell = 350$ and 352 for the FCM map) is presented in Fig. 6, where a structure that is perpendicular to the plane of the Galaxy and passes through its center is seen on the map. This was the first discovery of non-Gaussianity in the maps of the WMAP mission; such a non-Gaussianity is interpreted as the residual influence of the galactic background.

3.2 Circular statistical analysis and non-Gaussianity at multipoles with $10 \leqslant \ell \leqslant 50$

The phase properties of the WMAP maps were subsequently verified by other methods. The non-Gaussian properties of the CMB maps were demonstrated independently in Refs [81, 112] by analyzing the distributions of phases with the aid of cluster analysis and circular statistics, which deal with angles.

The phases of multipoles from the range $2 \leqslant \ell \leqslant \ell_{\max} = 50$ were examined for maps taken from the WMAP website. Besides the maps of background components prepared by the WMAP team for each observational frequency channel, five maps reflecting the difference between the signal in the observational channel (S) and the ILC signal, F = S − ILC, were also investigated in Refs [81, 112]. We call such maps 'secondary background maps', to distinguish them from those obtained by separating components and available on the WMAP site; the latter are called just the 'background maps'. If ψ_m and ϕ_m are the respective phases of a certain background component and of the ILC map for a given ℓ and all the corresponding values of m, then, according to the Fisher statistics [113] for angular quantities, we can define a circular cross-correlation coefficient for each mode ℓ:

$$R_{\rm sf}(\ell) = \ell^{-1} \sum_{m=1}^{\ell} \cos\left(\phi_m - \psi_m\right). \tag{13}$$

Figure 7 shows the calculated circular correlation coefficients between ILC data and background components, as well as between ILC and the secondary backgrounds for five frequency bands K – W. From the figure, it can be seen that for the first three channels, these coefficients are not large: they do not exceed the random spread (1σ) obtained in the case of 200 simulations. It is also seen that for all frequency bands, the functions $R_{\rm sf}(\ell)$ are similar to each other in shape, which reflects the strong correlations between phases in all channels [81]. Figure 7 also demonstrates that the correlation between ILC phases and the secondary background components looks more significant than in the case of WMAP backgrounds. Therefore, the behavior (position of maxima and minima) of the galactic background signal (without CMB) turns out to be coupled to the ILC CMB signal. The

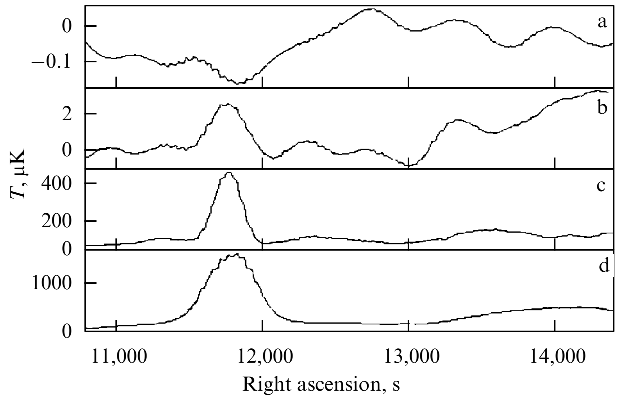

Figure 8. One-dimensional scans of WMAP maps: (a) ILC, (b) the radiation of dust in the W-channel, (c) free–free radiation in the V channel and (d) synchrotron radiation in the K-channel at the declination $\delta = 41°$ in the intersection region with the galactic plane (see peaks in Figs b–d).

manifestation of correlations is especially noticeable in the 11th multipole within the frequency bands Ka, Q, V, and W, and also in the entire W channel, where the radiation of dust is dominant. We note that the 11th multipole belongs to the range of spatial harmonics $10 \leqslant \ell \leqslant 20$, within which the radiation from the galactic plane, arriving from the region of angles $|b| < 10°$, is particularly significant. All the above points to the existence of a residual signal of galactic components in the cleaned CMB signal. The residual influence of the Galaxy on the cleaned signal can even be demonstrated by a one-dimensional scan, for example, at the declination $\delta = 41°$ (Fig. 8) [114], where a shallow temperature minimum is noticeable in the ILC map in the vicinity of the Galaxy.

3.3 Phase correlations between neighboring multipoles and random walk in phase space

To test the statistical independence of the phases $\phi_{\ell,m}$ for odd and even ℓ, trigonometric moments

$$\mathrm{Si}(\ell) = \ell^{-1} \sum_{m=1}^{\ell} \sin(\phi_{\ell,m}), \quad \mathrm{Ci}(\ell) = \ell^{-1} \sum_{m=1}^{\ell} \cos(\phi_{\ell,m}) \quad (14)$$

were used in [98] and the average angle for a given multipole ℓ was calculated as the arctangent of the ratio of the mean sine and cosine values for multipoles with fixed ℓ:

$$\Theta(\ell) = \arctan \frac{\mathrm{Si}(\ell)}{\mathrm{Ci}(\ell)} . \quad (15)$$

Here, in a homogeneous and isotropic random Gaussian field generated by primary fluctuations, homogeneity in the distribution of phases leads to homogeneity of the mean angles $\Theta(\ell)$ and to the absence of correlations between the angles $\Theta(\ell)$ characterizing multipoles of different ℓ. At the same time, such a correlation was found in [98]. First of all, the authors of [98] confirmed the coaxiality of the quadrupole and octupole components (see Section 6) manifested within the approach in Ref. [98] by the values of $\Theta(\ell)$ for $\ell = 2$ and $\ell = 3$ being close to each other. Moreover, they showed that such a fact (coaxiality) is not unique. For example, it was shown that a similar phenomenon of $\Theta(\ell)$ being close to each other is observed in the galactic coordinate system in the case of phases of certain multipole pairs with $\Delta\ell = 1$ (i.e., a correlation exists between neighboring even and odd multipoles, $\ell = 18.19$, 28.29, 33.34, etc.), and also with $\Delta\ell = 2$ ($\ell = 5.7$, 23.25, 33.35, etc.) in the ecliptic coordinate system.

Moreover, the authors of Ref. [98] proposed a random walk algorithm for the mean angles $\Theta(\ell)$ and revealed a significant discrepancy between the mean angle behavior in the case of even and odd harmonics, which is particularly clearly manifested in the ILC CMB map made in the galactic coordinate system. Along with the differences in the values of multipole coefficients C_ℓ for harmonics with even and odd ℓ, to be discussed in Section 10, this result points to spatial parity violation in the WMAP data. The authors of Ref. [98] explain the origin of the non-Gaussianity by both instrumental and possible cosmological reasons.

4. Instability of the reconstruction of the lower cosmic microwave background multipoles ($2 \leqslant \ell \leqslant 10$)

To understand the cross-correlation properties of the ILC background maps as a possible reason for non-Gaussianity, a numerical test [93] was performed using 10,000 simulations for the input CMB maps with a random Gaussian signal [86]. Starting from the 10,000 primary simulated CMB maps, the same number of maps in ΛCDM cosmology were obtained by adding the galactic background and further reconstructing the CMB by the ILC method (we call such maps output maps). Figure 9 shows histograms of the number of events $P(K_\ell)$ depending on K_ℓ, the correlation coefficient between the input (or output) map and the map of the background component for each simulation and each harmonic ℓ.

The shape of the distribution function for the input quadrupole component is in good agreement with the shape of the function $P(K) = A(1 - K^2)$, where A is a normalization factor. The dependence $P(K)$ shown in the upper-left coner of Fig. 9 ($\ell = 2$) is used in determining the first moment $\langle K \rangle = -0.00043$ and the second moment $\langle K^2 \rangle = 0.19934$ of $P(K)$ [115, 116]. A similar analysis can be performed for the output maps. From Fig. 9, it can be seen that the distribution function for the quadrupole is shifted significantly, with $\langle K \rangle \simeq -0.254$ for the dispersion $\sigma^2 = \langle K^2 \rangle - \langle K \rangle^2 \simeq 0.1454$. In the case of quadrupole and octupole components, not only is the center of gravity of the distribution function for the output signal shifted, but the shape of this function is also distorted. For $\ell = 4$, a virtually total correspondence is observed between the input and output maps. For the harmonics $\ell = 5$, 7, 9, a distortion of the distribution function is once again observed, which is due to the influence of background components. As can be seen from Fig. 9, application of the ILC method (to be more precise, the LILC method, which is one of the modifications of ILC [86] that reproduces the WMAP ILC map exactly) results in negative correlations with the background being obtained in the output maps with a higher probability than positive ones. The characteristic scales of differences between the input and output maps for the quadrupole and octupole components are comparable to the CMB signal itself. As shown in Ref. [117], these differences are related to the background components. To demonstrate the above, it is possible to use the WMAP data to calculate the combination $d_{\ell,m} = a^{(\mathrm{Ka})}_{\ell,m} - a^{(\mathrm{V})}_{\ell,m}$, to which only the background contributes, and to determine its correlation with the coefficients $a_{\ell,m}$ for the output LILC maps (for example, for simulated realization 00008 in [93]). In the case of even multipoles $\ell = 2, 4, 6, 8, 10$

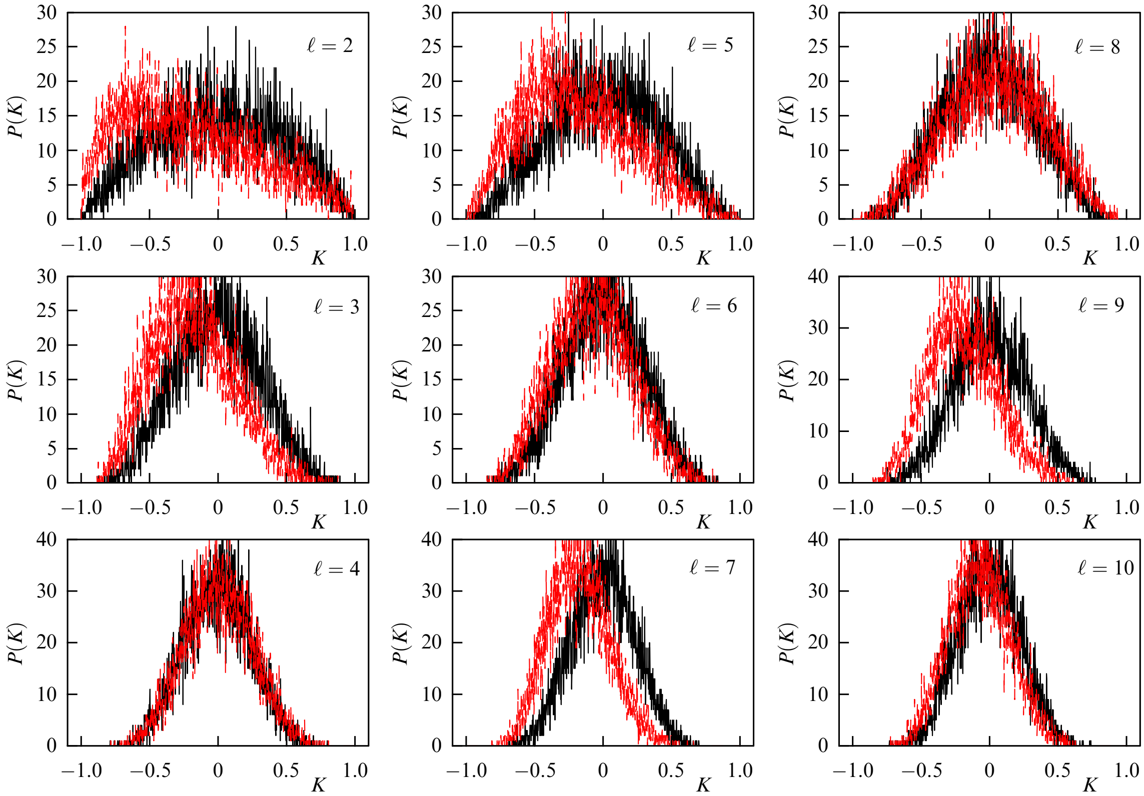

Figure 9. Distribution function $P(K)$ for the cross-correlation of random realizations of the CMB signal and the background component within the V band for $\ell = 2-10$, indicated in the figure. The dark solid line corresponds to the input signal and the light line to the output signal. (See also Ref. [93].)

pertaining to this CMB realization, the respective coefficients are $K_n^{\text{even}} = 0.183$, 0.421, 0.323, 0.136, 0.139, while for odd $\ell = 2n+1$, $n = 1, \ldots, 4$, $K_n^{\text{odd}} = 0.908$, 0.732, 0.732, 0.686. Thus, after reconstructing the octupole and other odd components, the signal is seen to be characterized by a high level of correlation with the background. Another important characteristic is the correlation of the residual map (obtained as the difference between the input and output maps) with the input one. In the case of even multipoles $\ell = 2n$ with $n = 1, \ldots, 5$, the respective coefficients are $K_n^{\text{even}} = -0.218$, -0.458, 0.0152, -0.223, -0.130, while for odd multipoles $\ell = 2n+1$ with $n = 1, \ldots, 4$, $K_n^{\text{odd}} = -0.172$, -0.116, -0.128, -0.011.

Moreover, the method described for testing the stability of the CMB signal reconstruction [93] revealed one more important peculiarity of the method for separating ILC components, which is related to the quadrupole problem. We use the same 10,000 input and output maps and examine the quadrupole mode $a_{2,0}$ applying the estimator $S = s_{2,0}^{\text{in}} s_{2,0}^{\text{out}}$, where $s_{2,0}^{\text{in,out}} = +1$ or -2 respectively for the positive or negative sign of the amplitude $a_{2,0}^{\text{in,out}}$ (the indices 'in' and 'out' are related to the input and output maps). If the signal is reconstructed correctly, we should have $S = +1$. But the value $S = -1$ is obtained for 2148 maps out of 10,000 simulated realizations. It can be assumed that such a strong effect is due to a change of the sign of $a_{2,0}$ in the case of those realizations for which it was primarily positive, $s_{2,0}^{\text{in}} = +1$, and that this change of sign is caused by an infiltration of the background signal. Indeed, in all background components within all frequency bands K–W of the WMAP mission, $a_{2,0}^{\text{f}}$ is negative, $s_{2,0}^{\text{f}} = -1$. If such an assumption is correct, a strong influence of the background on the characteristic discussed exists in the case of 43% of realizations that exhibit $s_{2,0}^{\text{in}} = +1$. We note that harmonics with an even value of $\ell + m$ are particularly difficult to reconstruct because the most powerful part of background components is concentrated in the galactic plane, and it mostly contributes to the modes with even values of $\ell + m$. It is also interesting to note that a forceful change of the sign in the quadrupole component alters the shape of the reconstructed quadrupole and resolves the issue of the existence of an 'axis of evil' [91]; from this standpoint, such a procedure is similar to modified methods for component separation [101].

5. Mosaic correlation

In Refs [118, 119], a mosaic correlation method is proposed for the analysis of a distributed signal, permitting one to reveal and investigate the possible residual influence of background components (both extended and determined by point sources) as the possible cause of non-Gaussianity within given regions for a given angular scale. The method has been realized in pixel parametric space. On the basis of a study of two maps with quite a high resolution and identical partitioning of the celestial sphere into pixels — maps of the temperature $\Delta T(\theta_i, \phi_i)$ and background radiation $S(\theta_i, \phi_i)$, where i is the pixel number — a mosaic correlation map of a lower resolution is made, where each pixel (which we call an M-pixel) contains a certain number of pixels of the primary maps. The M-pixel of a number p ($p = 1, 2, \ldots, N_0$, where N_0 is the total number of pixels on the sphere) is assigned the value of the correlation coefficient between the regions belonging to the two investigated higher-resolution maps and covered by this

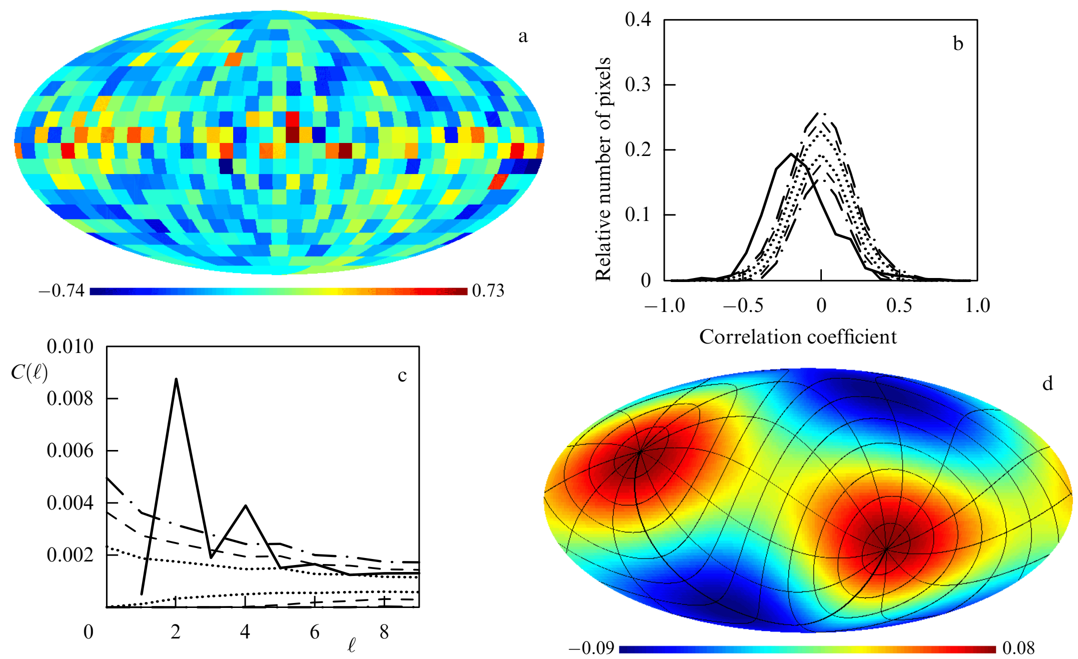

Figure 10. (See in color online.) Results of mosaic correlation between WMAP CMB ILC maps and maps of the background radiation of dust in the W channel with the correlation window $\Xi_p = 540' \times 540'$. (a) Mosaic map of M_c. (b) Histogram of the pixel distribution over correlation coefficients of the M_c map (solid curve). (c) Angular power spectrum of the M_c map. (d) Map of the quadrupole component of the M_c signal with a superposed grid of the equatorial coordinate system. The dotted, dashed, and dashed-dotted lines in Fig. b and c represent the respective spread levels of $\pm 1\sigma$, $\pm 2\sigma$, and $\pm 3\sigma$ in simulated mosaic maps of correlations calculated for 200 random Gaussian fields within the cosmological ΛCDM model. (See also Refs [118, 119].)

M-pixel. In other words, the correlation coefficient is calculated for two maps within the solid angle Ξ_p subtended by the given M-pixel. The solid angles Ξ_p are chosen to be identical and equal to Ξ for all M-pixels; the value of Ξ (the correlation window) determines the angular scale at which the correlation is studied. The total correlation coefficient for two primary maps at an angular scale Ξ has the form

$$K(\Xi) = \frac{1}{\sigma_{\Delta T_p} \sigma_{S_p}} \times \sum_p \sum_{(\theta_i, \phi_i) \in \Xi_p} \left(\Delta T(\theta_i, \phi_i) - \overline{\Delta T(\Xi_p)} \right) \left(S(\theta_i, \phi_i) - \overline{S(\Xi_p)} \right), \qquad (16)$$

where $\sigma^2_{\Delta T_p}$ and $\sigma^2_{S_p}$ are the dispersions.

This method permits checking the quality of the CMB component separation in the case of multifrequency observations, assuming the correlation between a random Gaussian signal of the CMB and the background components to be minimal. The presence of a residual correlated signal in the CMB data may lead to systematic errors in determining the angular power spectrum for different multipole ranges [93, 115] and, as a consequence, to a decrease in precision in determining cosmological parameters. Applying different correlation windows, we can see that in the distribution of correlation coefficients for WMAP ILC maps and the maps of background radiation of dust, there is, in the case of the correlation window $\Xi = 540' \times 540'$, a shift of -0.26 with respect to the expected zero value obtained by simulations with Gaussian smoothing in a window of radius 1° and of the masking of a region of the Galaxy. This is illustrated by Fig. 10, where the results are presented of a mosaic correlation of WMAP maps and of maps of the background radiation of dust (see Ref. [119] for the details). Besides the actual shift in the distribution of pixels over the correlation coefficients, a significant distortion of the shape of this distribution is to be noted. The medians of the pixel distributions for mosaic maps at correlation scales $160'$, $300'$, and $540'$ are respectively equal to -0.219, -0.233, and -0.274. It is interesting to note that the shift in the distribution of pixels of correlation maps is similar to the shift arising in the case of a nonstable reconstruction of the ILC signal in the quadrupole component [93].

The results of application of the above method in the case of WMAP CMB maps and of dust maps reveal the existence of a significant signal in the quadrupole component of the mosaic field, which leads to the appearance of a peak in the angular power spectrum. This peak is absent when calculations are performed of correlations between the map of simulated Gaussian perturbations and the radiation distribution of dust. The position of spots on the quadrupole map points to the presence of a signal related not only to the ecliptic coordinate system but also to the equatorial one, which is also observed when other methods are used [120, 121].

6. Multipole vectors

Already in Ref. [90], a correlation was noticed between the directions determined by the quadrupole and octupole CMB components (Fig. 11). A simple quantitative description of this phenomenon consists in finding a unit vector $\hat{\mathbf{n}}$ such that the projection of the angular momentum on it has the maximum dispersion, separately for the quadrupole and octupole. Specifically, we consider the contribution of

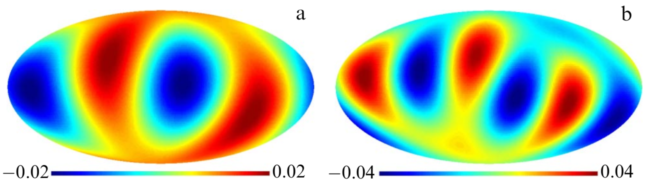

Figure 11. (See in color online.) The shape (a) of the quadrupole and (b) of the octupole in the WMAP ILC map based on data obtained during the seventh year of observations.

multipoles with a given ℓ to the anisotropy of the CMB temperature:

$$\Delta T_\ell(\theta,\phi) = \sum_{m=-\ell}^{\ell} a_{\ell m} Y_{\ell m}(\theta,\phi)\,, \tag{17}$$

and construct the dispersion as a function of the direction of $\hat{\mathbf{n}}$:

$$\left\langle \Delta T_\ell\,(\hat{\mathbf{n}}\mathbf{L})^2 \Delta T_\ell \right\rangle = \sum_{m=-\ell}^{\ell} m^2 \left|a_{\ell m}(\hat{\mathbf{n}})\right|^2, \tag{18}$$

where $\mathbf{L}$ is the angular momentum operator, the angular brackets indicate averaging over the celestial sphere, and the coefficients $a_{\ell m}(\hat{\mathbf{n}})$ are calculated in a coordinate system with the third axis coinciding with $\hat{\mathbf{n}}$. Using the data obtained by the WMAP mission during its first year of work, the authors of Ref. [90] found the vectors determining the maxima of dispersion for the quadrupole and for the octupole to be quite close to each other:

$$\hat{\mathbf{n}}_2 = (-0.1145, -0.5265, 0.8424)\,,$$
$$\hat{\mathbf{n}}_3 = (-0.2578, -0.4207, 0.8698)\,.$$

The scalar product of these vectors, which could be any number in the interval $(0, 1)$ [dispersion (18) does not change when the sign of $\hat{\mathbf{n}}$ changes, and therefore the product $\hat{\mathbf{n}}_2\hat{\mathbf{n}}_3$ can be considered positive], is

$$\hat{\mathbf{n}}_2\hat{\mathbf{n}}_3 = 0.9838\,.$$

The probability of such a coincidence occurring in the case of a Gaussian map was estimated by the authors of Ref. [90] to be 1/60.

For a more detailed study of the issue of coaxiality of multipoles, Copi and co-authors [122, 123] proposed using the formalism of multipole vectors first introduced by Maxwell [124], and applied it in investigating the CMB anisotropy at large scales. A property of these vectors is their independence from the choice of the coordinate system, which renders them applicable in tests of the zero statistical isotropy hypothesis and in searches for directions in the sky along which manifestations of non-Gaussianity can occur due to various reasons: nonstandard physics, the existence of systematic errors, the residual influence of background components, the topology of the Universe, and so on [94].

Following [123], the contribution of multipoles with a given ℓ to the anisotropy of the CMB temperature can be represented in a form equivalent to (17),

$$\Delta T_\ell(\theta,\phi) = \sum_{i_1,\ldots,i_\ell} K_{i_1,\ldots,i_\ell}\, e_{i_1}(\theta,\phi)\ldots e_{i_\ell}(\theta,\phi)\,,$$

where the spatial indices i_α range values from 1 to 3, $\mathbf{e}(\theta,\phi) = (\sin\theta\cos\phi, \sin\theta\sin\phi, \cos\theta)$ is a unit three-dimensional vector directed along (θ,ϕ) on the sphere, and $K_{i_1,\ldots,i_\ell}$ is a traceless symmetric real tensor of rank ℓ in three-dimensional space. This tensor, as well as the set of amplitudes $a_{\ell m}$, has $2\ell+1$ independent real components. The idea consists in writing this tensor in the form of a combination of ℓ unit real three-dimensional vectors $\mathbf{v}^{(\ell,\alpha)}$, $\alpha = 1,\ldots,\ell$ (2ℓ independent components altogether) and an overall amplitude A_ℓ:

$$K_{i_1,\ldots,i_\ell} = A_\ell\big[v_{i_1}^{(\ell,1)}\cdots v_{i_\ell}^{(\ell,\ell)}\big]_{\mathrm{TF}}\,,$$

where $[\ldots]_{\mathrm{TF}}$ denotes taking the symmetric traceless part. It is known that such a representation exists and that it is unique, and therefore the set of unit vectors $\mathbf{v}^{(\ell,\alpha)}$, together with the amplitude A_ℓ, fully characterizes the multipole component $\Delta T_\ell(\theta,\phi)$. We note that vectors $\mathbf{v}^{(\ell,\alpha)}$ are defined up to their signs, because a change of sign of each of these vectors can be compensated by a change of sign of the amplitude A_ℓ. We also note that multipole vectors are independent of the total power C_ℓ of the temperature multipole with a fixed ℓ: if all the $a_{\ell m}$ for a given ℓ are additionally multiplied by a common factor, then A_ℓ is also multiplied by this factor, while $\mathbf{v}^{(\ell,\alpha)}$ remains unchanged. In particular, if the quantity $\tilde{a}_{\ell m} = a_{\ell m}/\sqrt{C_\ell}$ is used, the multipole vectors $\mathbf{v}^{(\ell,\alpha)}$ depend only on $\tilde{a}_{\ell m}$, but not on C_ℓ. In this sense, multipole vectors carry information complementary to the information encoded in the angular power spectrum, and no assumptions concerning the non-Gaussianity or statistical isotropy have any influence here.

A relatively simple algorithm for finding multipole vectors was proposed in Ref. [122], where, given the coefficients $a_{\ell m}$, the multipole vectors are constructed using a standard harmonic expansion. The complete calculations, along with recurrence formulas for $\mathbf{v}^{(\ell,\alpha)}$ within this approach, are presented in Ref. [122]. A program code with open access also exists.[4]

The area vectors

$$\mathbf{w}^{(\ell,\alpha\beta)} = \mathbf{v}^{(\ell,\alpha)} \times \mathbf{v}^{(\ell,\beta)}$$

were also introduced in [94, 123]. These vectors are orthogonal to the planes of the ℓ-multipole in which the pairs of vectors $(\mathbf{v}^{(\ell,\alpha)}, \mathbf{v}^{(\ell,\beta)})$ lie, and are also defined up to their signs. In the case of the quadrupole, there are two multipole vectors, $\mathbf{v}^{(2,1)}$ and $\mathbf{v}^{(2,2)}$, and only a single area vector $\mathbf{w}^{(2,12)}$; an octupole is characterized by three multipole vectors and three area vectors.

The observation made in Refs [94, 123] is that the quadrupole and octupole planes are close to each other, i.e., the directions of the vectors $\mathbf{w}^{(2,12)}$, $\mathbf{w}^{(3,12)}$, $\mathbf{w}^{(3,13)}$, and $\mathbf{w}^{(3,23)}$ are correlated at a confidence level exceeding 99%. To be more precise, the vector $\mathbf{w}^{(2,12)}$ lies nearly in the middle between the three vectors $\mathbf{w}^{(3,12)}$, $\mathbf{w}^{(3,13)}$, and $\mathbf{w}^{(3,23)}$, while the results in Ref. [94] lead to the following for the scalar products (data obtained by the WMAP during three years of work were used):

$$\frac{\mathbf{w}^{(2,12)}\,\mathbf{w}^{(3,12)}}{|\mathbf{w}^{(2,12)}||\mathbf{w}^{(3,12)}|} = 0.858\,, \qquad \frac{\mathbf{w}^{(2,12)}\,\mathbf{w}^{(3,13)}}{|\mathbf{w}^{(2,12)}||\mathbf{w}^{(3,13)}|} = 0.804\,,$$
$$\frac{\mathbf{w}^{(2,12)}\,\mathbf{w}^{(3,23)}}{|\mathbf{w}^{(2,12)}||\mathbf{w}^{(3,23)}|} = 0.872\,.$$

[4] http://www.phys.cwru.edu/projects/mpvectors/

All these quantities are close to unity, which precisely signifies the coaxiality of the quadrupole and octupole. We note that the octupole vectors $\mathbf{w}^{(3,12)}$, $\mathbf{w}^{(3,13)}$, and $\mathbf{w}^{(3,23)}$ are also close to one another ('planarity' of the octupole).

Moreover, all four area vectors are correlated with the ecliptic plane and (at a confidence level exceeding 95%) with the direction of the dipole and the positions of the equinoctial points. All the above seems to contradict the assumption of Gaussianity and the statistically isotropic ILC map.

7. Quadrupole statistical anisotropy

Some inflationary models with vector fields predict that primary scalar perturbations are Gaussian, but statistically anisotropic. This means that their power spectrum should depend not only on the length of the wavevector but also on its direction $\hat{\mathbf{k}} = \mathbf{k}/k$:

$$\left\langle \Phi(\mathbf{k})\Phi^*(\mathbf{k}')\right\rangle = P(k)\,\delta(\mathbf{k}-\mathbf{k}')\left[1+g(k,\hat{\mathbf{k}})\right]. \tag{19}$$

For example, a quite well-reasoned dependence is given in [25–28]:

$$g(k,\hat{\mathbf{k}}) = g_0(\hat{\mathbf{k}}\hat{\mathbf{N}})^2\,, \tag{20}$$

where $\hat{\mathbf{N}}$ is a certain fixed unit vector constant in space and g_0 is a constant. Models based on conformal invariance predict statistical anisotropy of a more general form [56, 57].

Statistical anisotropy of form (19) would be manifested in the CMB signal as nonzero correlators of multipoles with different (ℓ, m) [cf. formula (6) for statistically isotropic perturbations]:

$$\langle a_{\ell m} a^*_{\ell' m'}\rangle \neq 0 \quad \text{for} \quad \ell \neq \ell' \quad \text{and/or} \quad m \neq m'\,.$$

A method for searching for this effect was developed in Refs [125, 126].

Statistical anisotropy in form (20) was indeed discovered in the WMAP CMB data [126–128] (see also Ref. [69]). Here,

$$g_0 = 0.29 \pm 0.03\,,$$

i.e., the signal is large in amplitude and is statistically significant. But the direction of the vector $\hat{\mathbf{N}}$, namely, $(b,l) = (30°, 96°)$, turned out to be close to the normal of the ecliptic plane. This is a serious indication that the effect is due to systematic errors. Most probably, it can be explained by an asymmetry in the polar pattern of the WMAP receivers [127] (the authors of [128] do not agree with this interpretation, however).

8. Minkowski functionals

Minkowski functionals [129] are an effective tool for investigating the morphology of sets of regions in space (regions on the celestial sphere in the case of the CMB). These functionals are actively used in studies of the statistics of a signal. The historical aspects and the algorithmic details of this method are described in book [48]. We briefly note that the three-dimensional version of the method was applied in cosmology back in the 1990s in studies of the distribution of objects in the Universe [130, 131]. The idea of using morphological characteristics of a map for describing the statistical properties of the CMB signal anisotropy has been described and developed in a series of publications [48, 132–138].

It is convenient to choose the following field of unit dispersion as the quantity to be considered, instead of temperature:

$$v(\theta,\phi) = \frac{\Delta T(\theta,\phi)}{\sigma_0}\,,$$

where σ_0 is the dispersion of temperature fluctuations,

$$\sigma_0^2 = \langle \Delta T^2\rangle = \frac{1}{4\pi}\sum_{\ell}(2\ell+1)\,C(\ell)\,. \tag{21}$$

As before, the angular brackets denote averaging over the celestial sphere. We now fix a certain value of v, and for a given map construct all the connected regions $R_i(v)$ on a unit celestial sphere inside which $v(\theta,\phi) > v$. Generally speaking, the regions $R_i(v)$ are not singly connected, i.e., they may have holes in them [and inside these holes there may in turn be regions with $v(\theta,\phi) > v$, which must also be included in the set $\{R_i(v)\}$]. It is possible to define three global (i.e., relevant to the entire sphere) Minkowski functionals:

(1) the normalized area

$$A(v) = \frac{1}{4\pi}\sum_i A\left[R_i(v)\right],$$

where $A[R]$ is the area of region R;

(2) the total normalized length of isolines

$$L(v) = \frac{1}{4\pi}\sum_i L\left[R_i(v)\right],$$

where $L[R]$ is the length of the perimeter of region R;

(3) the genus $G(v)$ — the difference between the number of connected regions with $v(\theta,\phi) > v$ and the number of connected regions with $v(\theta,\phi) < v$ (a quantity equivalent to the genus is the Euler characteristic).

It is remarkable that these three functionals fully describe the morphology of the set of regions $\{R_i(v)\}$ (in a d-dimensional space, there are $d+1$ such functionals). In a similar manner, it is possible to define three local Minkowski functionals relevant to an individual part of the sphere, instead of the whole sphere.

In the analysis of the CMB, another characteristic is often used instead of the genus:

$$\tilde{G}(v) = N_{\max}(v) + N_{\min}(v) - N_{\text{sad}}(v)\,,$$

where $N_{\max}(v)$, $N_{\min}(v)$, and $N_{\text{sad}}(v)$ are the numbers of maxima, minima, and saddle points of the function $v(\theta,\phi)$ in all the regions $R_i(v)$. For the sphere, $G(v) = \tilde{G}(v) - 1$.

In the case of a Gaussian field, the global Minkowski functionals can be calculated analytically. On a plane, the normalized functionals are expressed as [48]

$$\begin{aligned} A(v) &= \frac{1}{2} - \frac{1}{2}\,\Phi\left(\frac{v}{\sqrt{2}}\right), \\ L(v) &= \frac{1}{8\theta_{\text{c}}}\exp\left(-\frac{v^2}{2}\right), \\ G(v) &= \frac{1}{(2\pi)^{3/2}}\,\frac{1}{\theta_{\text{c}}^2}\exp\left(-\frac{v^2}{2}\right), \end{aligned} \tag{22}$$

where

$$\Phi(x) = \frac{2}{\sqrt{\pi}} \int_0^x \exp(-x^2)\, dx$$

is the error function and θ_c is the correlation length of the field defined as

$$\theta_c^{-1} = \sqrt{\frac{\left\langle (\nabla \Delta T)^2 \right\rangle}{\langle \Delta T^2 \rangle}} = \frac{\sigma_1}{\sigma_0}\,,$$

where σ_1 is the dispersion of the temperature gradient,

$$\sigma_1^2 = \frac{1}{4\pi} \sum_{\ell} \ell(\ell+1)(2\ell+1)C(\ell)\,. \tag{23}$$

Thus, it is possible to search for deviations from Gaussianity by checking whether relations such as (22) are satisfied.

Minkowski functionals have been used in verifying the Gaussianity of WMAP data. The three functionals described above, as well as a number of other characteristics, were used in [85] in analyzing the CMB maps obtained by the WMAP mission during its first year of observations; the results were compared with those of Gaussian perturbation simulations with the WMAP noise signal. The authors of Ref. [85] found that in the analysis of the whole sphere at angular scales between 1° and 4°, all sorts of statistics are generally consistent with the assumed Gaussianity of the CMB signal. At the same time, it was shown that the properties of CMB arriving from the northern and southern Galactic hemispheres differ significantly. The statistics of the signal from the southern hemisphere at the $1° - 4°$ angular scales studied is, on the whole, consistent with the Gaussianity hypothesis, while in the case of the northern hemisphere, a number of peculiarities are observed. Although the area and length functionals $A(v)$ and $L(v)$ are quite consistent with the Gaussianity hypothesis, the genus of the northern hemisphere exceeds the expected value at all angular scales, and at the scale of 3.4°, its amplitude is so high that only one of the 5000 realizations has a higher amplitude for negative threshold values v. Moreover, using the statistics introduced in Ref. [139] (the length of the skeletal line), as well as other statistics, the authors of Ref. [85] found the values of the parameter to be

$$\gamma = \frac{\sigma_1^2}{\sigma_0 \sigma_2}\,,$$

where σ_0 and σ_1 are the respective dispersions of temperature and its gradient, defined by (21) and (23), and σ_2 is the dispersion of the second-order derivatives, which is defined quite similarly. In 99% of simulations for the northern hemisphere, the parameter γ exceeded the expected value, while no such effect was observed for the southern hemisphere. We note that before paper [85] was published, an asymmetry between the genus amplitudes for the northern and southern hemispheres had already been reported in [84]. However, the results in [84] were obtained for significantly smaller angular scales than in Ref. [85], and it is therefore difficult to establish any direct relation between these two groups of results. In any case, investigation of the Minkowski genus has demonstrated that the Gaussian model of fluctuations encounters difficulties in describing the WMAP data at large and intermediate angular scales.

Minkowski functionals have also been used to estimate the parameter f_{NL} [140] in the model of non-Gaussian primary perturbations described by formula (8). For this, the authors generated CMB maps in the framework of that model and considered their difference from maps calculated within the model with Gaussian primary inhomogeneities (actually, as underlined by the authors, at not too large values of f_{NL}, the expressions for Minkowski functionals in the non-Gaussian model can be obtained with good precision analytically). The authors also took various observational effects complicating the situation into account, such as the function of a pixel window, 'blurring' by the polar diagram, inhomogeneous noise, and screening masks on the map. On the basis of the behavior of Minkowski functionals at different scales and at different levels of non-Guassianity in model maps, the authors of Ref. [140] obtained constraints on the non-Gaussianity level for the data obtained by the WMAP mission during its third year of work, namely, they obtained the estimate $-70 < f_{\mathrm{NL}} < 91$ at a 95% confidence level from maps made of combined data from $\mathrm{Q}+\mathrm{V}+\mathrm{W}$ channels of the WMAP mission smoothed out by a Gaussian filter at scales of $10'$, $20'$, and $40'$. For the combination of $\mathrm{V}+\mathrm{W}$ maps, the obtained estimate $-108 < f_{\mathrm{NL}} < 64$ was shifted into the region of negative values, and it differed, for example, from the limit values f_{NL} shifted into the region of positive values, $27 < f_{\mathrm{NL}} < 147$, and found in Ref. [141] for the same data with the aid of the bispectrum.

9. Spherical wavelets

9.1 Non-Gaussian kurtosis

Among the first searches for non-Gaussianity in the WMAP CMB data, there is a series of studies based on the analysis by means of wavelets [83, 142]. The first attempts to apply this technique in searching for non-Gaussian features were made in the 1990s with the COBE–DMR (COsmic Background Explorer–Differential Microwave Radiometer) data [143] with the aid of Daubechies wavelets, and later with the aid of spherical wavelets (Spherical Haar Wavelet — SHW) [144]. 'Spherical mexican hat' wavelets (SMHWs) are the most sensitive to manifestations of non-Gaussianity [145–147].

SMHWs can be constructed with the aid of a Euclidean wavelet of the Mexican hat type (Mexican hat wavelet, MHW) using the stereographic projection proposed in Ref. [148]. A SMHW depends on three parameters: the general scale R and the coordinates (θ, ϕ) of a point on the sphere playing the role of the pole relative to which the stereographic projection is realized. For each choice of the wavelet center, it is convenient to introduce a new coordinate system (with primed coordinates), whose center is the north pole. Then the explicit form of the SMHW wavelet is

$$\Psi_{\mathrm{S}}(y, R) = \frac{1}{\sqrt{2\pi}\, N(R)} \left[1 + \left(\frac{y}{2}\right)^2\right]^2 \left[2 - \left(\frac{y}{R}\right)^2\right] \exp\left(-\frac{y^2}{2R^2}\right), \tag{24}$$

where

$$N(R) = R\left(1 + \frac{R^2}{2} + \frac{R^4}{4}\right)^{1/2} \tag{25}$$

is a normalization factor. The distance on the tangent plane is given by the quantity y that is related to the polar angle as

$$y = 2\tan\frac{\theta'}{2}\,,$$

where θ' is the polar angle in the primed coordinate system. The expansion of temperature fluctuations in wavelets has the standard form

$$w(R;\theta,\phi) = \int \sin\theta'\,\mathrm{d}\theta'\,\mathrm{d}\phi'\,\Psi_S(R;\theta')\,\Delta T(\theta',\phi')\,,$$

where the temperature is assumed to be reduced to the primed coordinate system (precisely for this reason, w depends on θ and ϕ). In practice, a finite number of wavelet centers are chosen for each scale R, i.e., the wavelet expansion $w_i(R) \equiv w(R;\theta_i,\phi_i)$, $i = 1,\ldots,N_R$, is restricted to a finite number of coefficients.

The coefficients of the wavelet expansion $w_i(R)$ are expressed linearly in terms of temperature fluctuations. Therefore, in the case of the Gaussian CMB signal, these coefficients must also exhibit Gaussian statistics. To search for deviations from Gaussianity at a given scale R, several quantities can be determined. In [83], two simple estimators of non-Gaussianity were used: the skewness $S(R)$ and the kurtosis $K(R)$:

$$S(R) = \frac{1}{N_R}\sum_{i=1}^{N_R}\frac{w_i^3(R)}{\sigma^3(R)}\,, \tag{26}$$

$$K(R) = \frac{1}{N_R}\sum_{i=1}^{N_R}\frac{w_i^4(R)}{\sigma^4(R)} - 3\,, \tag{27}$$

where N_R is the number of wavelet coefficients on the scale R and $\sigma(R)$ is the dispersion of wavelet coefficients on this scale:

$$\sigma^2(R) = \frac{1}{N_R}\sum_{i=1}^{N_R} w_i^2(R)\,. \tag{28}$$

Using this approach, the authors of Ref. [83] obtained an excess of the kurtosis $K(R)$ on two successive scales, $R_8 = 4.17°$ and $R_9 = 5°$, in the WMAP CMB data. The kurtosis at $R_8 = 4.17°$ is only realized in 40 cases out of 10,000 for Monte Carlo simulations, which the authors consider an indication of the non-Gaussianity of the WMAP map. A similar result is also true for the scale R_9. The authors of [83] found a non-Gaussian signal in the entire frequency range of the WMAP mission (from 23 to 94 GHz) and showed its frequency independence. It was also shown that after the addition of a contamination signal in the form of an overestimated background, no non-Gaussian signal was revealed by the simulated Gaussian CMB maps. It was therefore concluded in [83] that the addition of the galactic background to CMB models does not give rise to non-Gaussianity if searches are based on the wavelet analysis, and that galactic background components are not the source of the discovered non-Gaussianity of the ILC CMB map. Moreover, the application of this method has shown that the signal in the northern hemisphere is consistent with the Gaussian model, while in the southern hemisphere, as on the entire sphere, the CMB data exhibit non-Gaussianity.

9.2 Cold Spot

A cold region (Fig. 12) exhibiting a complex structure was identified in the CMB in [142] using SMHWs. The non-Gaussianity of the signal in the southern hemisphere was explained in [142] precisely by the existence of this region. The galactic coordinates of this region, called the Cold Spot (CS), are $b = -57°$, $l = 209°$. The probability of the signal distribution being consistent with the Gaussian model, if SMHWs are used, amounts to about 0.2% [142]. The frequency dependence of the signal in the CS region is similar to the one in other CMB spots. The authors also found that if that zone is removed, the remaining set of data corresponds to Gaussian assumptions in the SMHW analysis.

It must be noted, however, that the conclusions in [150] were criticized in [150], because the use of weight functions differing from SMHWs (in particular, by Gaussian weights of variable width) does not lead to the revelation of any signal non-Gaussianity. Thus, the problem of the CS statistical significance has not yet been fully resolved.

After obtaining indications of the signal non-Gaussianity at the Cold Spot, as well as messages on the reduced density of sources [151] in smoothed-out maps of the radio survey NVSS (NRAO (National Radio Astronomy Observatory) VLA (Very Large Array) Sky Survey) [152] (which also gave rise to doubt [153], however), several hypotheses concerning the origin of the Cold Spot were put forward, which were related to the integrated Sachs–Wolfe effect [151], the topological defect [39], the artefact of data analysis [154], and simply a random deviation [155, 156]. We note that such a spot in the WMAP CMB map is not unique [154, 155], and that its properties are mainly determined by low harmonics ($2 \leqslant \ell \leqslant 20$). The statistics of extragalactic objects in the CS region in various wavelength ranges does not differ within the uncertainty from the statistics of other regions in the given band of galactic latitudes [157]. There are other spots whose non-Gaussian properties also depend on low ℓ [158]. Moreover, another interesting point presented in Ref. [154] must be

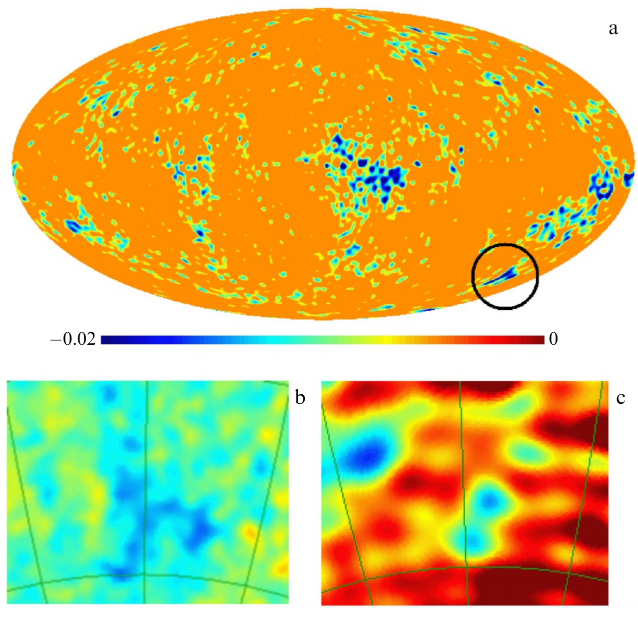

Figure 12. (a) Position of the non-Gaussian Cold Spot on the sphere in galactic coordinates. (b) Cold Spot on the ILC WMAP close-up map. (c) Cold zone on a map for the 408 MHz frequency channel in 1982 [149].

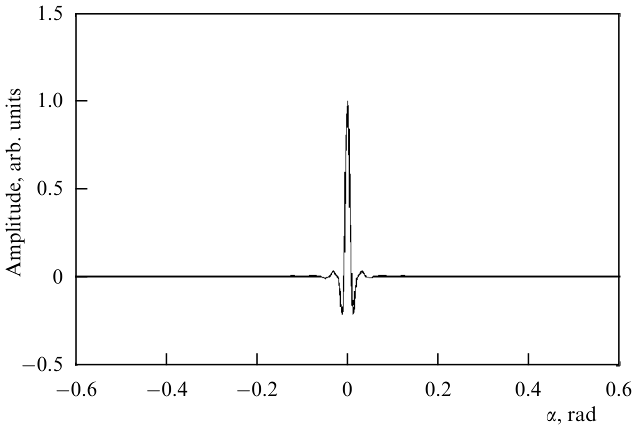

Figure 13. Example of a needlet with $B = 2$ and $j = 8$ in pixel space [162]; α is the removal angle from the function maximum.

noted; the CS is also manifested in the data of 1982 in maps of a low-frequency (408 MHz) survey [149] (see Fig. 12), where synchrotron radiation contributes significantly to the background.

9.3 Needlets

To conclude this section, we mention the second generation of spherical wavelets, namely, needlets, which were introduced into functional analysis in [159, 160] (Fig. 13). A spherical needlet is defined as [161]

$$\psi_{jk}(\theta,\phi) = \sqrt{\lambda_{jk}} \sum_{\ell} b\left(\frac{\ell}{B^j}\right) \sum_{m=-\ell}^{\ell} Y^*_{\ell m}(\theta,\phi)\, Y_{\ell m}(\theta_k,\phi_k)\,, \quad (29)$$

where (θ,ϕ) are coordinates on the sphere, j is the number of the needlet harmonic, and λ_{jk} is a normalization factor. The points (θ_k,ϕ_k) that are needlet vertices may coincide with pixel centers within the given pixelization scheme. The number B fixes a needlet basis such that it only involves multipoles from the range $\ell \in [B^{j-1}, B^{j+1}]$, i.e., the function $b(\ell/B^j)$ corresponds to the window function and is equal to zero outside the range $[B^{j-1}, B^{j+1}]$ [162].

The approach involving needlets was used for estimating the primary non-Gaussianity, characterized by the parameter f_{NL}, with the aid of a needlet bispectrum [161]. The advantage of this approach compared to the usual approach using harmonic bispectrum (7) consists in the more correct work with regions covered by masks. The estimate of f_{NL} obtained in Ref. [161] with the influence of point sources taken into account is $f_{\mathrm{NL}} = 84 \pm 40$.

10. Angular power spectrum

A remarkable manifestation of non-Gaussian properties of the WMAP CMB map consists in parity asymmetry, first noticed in [97]. The simplicity of the approach proposed in [97] is related to the possibility of only using the CMB angular power spectrum C_ℓ, without having to use maps and individual harmonics $a_{\ell m}$. For a Gaussian random field of primary perturbations $\Phi(\mathbf{k})$ with a flat power spectrum, the presence of a plateau in the CMB angular power spectrum is expected at low multipoles, which is due to the Sachs–Wolfe effect, namely, to the fact that $\ell(\ell+1)C_\ell \approx$ const. Spherical harmonics change as $Y_{\ell m}(\hat{\mathbf{n}}) = (-1)^\ell Y_{\ell m}(-\hat{\mathbf{n}})$ when the coordinates are reversed. Therefore, an asymmetry in the angular power spectrum for even and odd harmonics can be regarded as the asymmetry of the power of even and odd components of maps. The authors of Ref. [97] found the power of odd multipoles to systematically exceed the power of even multipoles of low ℓ and termed this phenomenon 'parity asymmetry'. To describe such an asymmetry quantitatively, the following quantities are proposed for consideration:

$$P^+ = \sum_{\text{Even } \ell<\ell_{\max}} \frac{\ell(\ell+1)C_\ell}{2\pi}\,,$$

$$P^- = \sum_{\text{Odd } \ell<\ell_{\max}} \frac{\ell(\ell+1)C_\ell}{2\pi}\,.$$

Using the data of the WMAP power spectrum and the results of Monte Carlo simulations, the authors of Ref. [97] calculated the ratio P^+/P^- for the multipole ranges $2 \leqslant \ell \leqslant \ell_{\max}$, where $\ell_{\max}$ lies between 3 and 23. Comparing P^+/P^- for the WMAP data with the similar ratio obtained for simulated maps allows estimating the quantity p equal to the fraction of simulated spectra in which P^+/P^- is less than or equal to the same quantity for the WMAP map. The value of p was found to reach its lower boundary at $\ell_{\max} = 18$, where p equals 0.004 and 0.001 for the data obtained by the WMAP mission during five and three years of observations, respectively. This fact means that there is a preference for odd multipoles ($2 \leqslant \ell \leqslant 18$) in the WMAP data at a confidence level of 99.6% with a screening mask imposed on the data, and of 99.76% without any mask. The authors believe the low amplitude of the WMAP CMB quadrupole may be part of the same anomaly as the parity asymmetry. Because the power asymmetry of the CMB signal in the northern and southern hemispheres is manifested more strongly in the case of multipoles with $2 \leqslant \ell \leqslant 19$ than multipoles with $20 \leqslant \ell \leqslant 40$ [86], the authors of Ref. [97] also believe that the general origin of anomalies (such as the power asymmetry in the hemispheres, the low quadrupole amplitude, and the parity asymmetry) lie in the region of small ℓ and that the explanation can be either cosmological or related to the presence of systematic errors in observations that were not revealed and/or were additionally introduced in the course of analysis of the data obtained by the WMAP mission.

11. Conclusion

In this article, we have described certain tests that have been extensively used during the past decade in searches for and studies of non-Gaussianity and statistical anisotropy of CMB data differing in nature.

It is necessary to make several general comments concerning the methods described.

• As was shown for different ranges of multipoles in a large number of studies, there are indications that the WMAP CMB data exhibit deviations from Gaussianity, revealed with the aid of methods involving phase analysis, cross-correlations with galactic background components, spherical wavelets, Minkowski functionals, angular power spectra, etc.

• Different methods for testing non-Gaussian properties are sensitive to different types of non-Gaussianity manifestation. For example, phase analysis 'sees' residual manifestations due to galactic background components (or systematic errors) in the cleaned CMB signal, while at the same time the bispectrum and other similar methods are not sensitive to this type of non-Gaussianity.

• Low multipoles of the WMAP CMB data exhibit deviations from Gaussianity and/or statistical isotropy practically independently of which method is used for testing this phenomenon.

• The level of primary non-Gaussianity of certain types, for example, the one described by the parameter $f_{\rm NL}$, is estimated by methods that are insensitive to the residual galactic background. For example, if a background spot is 'shifted' without changing its size, it is possible to obtain a map with a signal distribution that is Gaussian, determined from the temperature distribution but with connected phases of different multipoles.

• Simulation in the framework of the ideas of Gaussian and statistically isotropic primary perturbations and standard ΛCDM cosmology serves as an important tool for understanding the observational process, analyzing data, and estimating the confidence level. Simulations involving non-Gaussian and/or statistically anisotropic primary perturbations under certain concrete assumptions concerning their properties are also useful. However, if the CMB has non-Gaussian properties of another, as yet unrevealed, nature differing from the one inherent in the model, the use of the latter approach may impose restrictions on our interpretation of the data.

• We have at our disposal a sole realization of data from the real CMB, whose characteristics are certainly not known because the true CMB signal is screened by the galactic background, smoothed out by the non-Gaussian beam pattern, and added up with the noise. For any single, even Gaussian, CMB realization, it is in principle possible to choose a test that would reveal its 'false' non-Gaussianity, already because, first, observations provide a limited set of data and, second, these data are taken from the primary array, which is certain to contain non-Gaussian systematic errors and contributions from background radiation. The issue of the correct estimation of the statistical reliability of peculiarities revealed a posteriori is still under debate.

The prospects for developments along the line of research discussed in this article are related to enhancement of the precision of experiments and to an even more accurate estimation of contamination factors that reduce our dependence on the a priori information in the course of Monte Carlo simulations. Experiments exhibiting high sensitivity, such as the Planck mission covering a broad range of frequencies and having better resolution, will permit checking the results obtained by the WMAP mission and will probably correct the results of searches for primary non-Gaussianity.

Acknowledgements

The author is grateful to his colleagues A G Doroshkevich and P D Naselsky for the fruitful discussions of non-Gaussianity. The author expresses personal acknowledgment to V A Rubakov for reading the manuscript and for the discussions and comments owing to which the text of the article was significantly improved and certain sections were essentially extended, in particular, Sections 1 and 6, as well as the list of references, and Section 7 was additionally written. In this work, we used the open archive of observations of the WMAP NASA mission; for data analysis and construction of the CMB image, the GLESP (Gauss-Legendre Sky Pixelization)[5] package [163, 164] was used. The author is grateful to the Dmitrii Zimin Foundation of Noncommercial Programs 'Dynasty' and to the RFBR (grant 09-02-00298) for support.

References

1. Starobinskii A A *Pis'ma Zh. Eksp. Teor. Fiz.* **30** 719 (1979) [*JETP Lett.* **30** 682 (1979)]
2. Sato K *Mon. Not. R. Astron. Soc.* **195** 467 (1981)
3. Guth A H *Phys. Rev. D* **23** 347 (1981)
4. Albrecht A, Steinhardt P J *Phys. Rev. Lett.* **48** 1220 (1982)
5. Linde A D *Phys. Lett. B* **108** 389 (1982)
6. Mukhanov V F, Chibisov G V *Pis'ma Zh. Eksp. Teor. Fiz.* **33** 549 (1981) [*JETP Lett.* **33** 532 (1981)]
7. Hawking S W *Phys. Lett. B* **115** 295 (1982)
8. Starobinsky A A *Phys. Lett. B* **117** 175 (1982)
9. Guth A H, Pi S-Y *Phys. Rev. Lett.* **49** 1110 (1982)
10. Bardeen J M, Steinhardt P J, Turner M S *Phys. Rev. D* **28** 679 (1983)
11. Allen T J, Grinstein B, Wise M B *Phys. Lett. B* **197** 66 (1987)
12. Linde A, Mukhanov V *Phys. Rev. D* **56** R535 (1997)
13. Bernardeau F, Uzan J-P *Phys. Rev. D* **66** 103506 (2002)
14. Dvali G, Gruzinov A, Zaldarriaga M *Phys. Rev. D* **69** 023505 (2004); astro-ph/0303591
15. Kofman L, Report CITA-03-12; astro-ph/0303614
16. Barnaby N, Cline J M *Phys. Rev D* **75** 086004 (2007); astro-ph/0611750
17. Falk T, Rangarajan R, Srednicki M *Astrophys. J.* **403** L1 (1993)
18. Maldacena J *JHEP* (05) 013 (2003)
19. Salopek D S, Bond J R *Phys. Rev. D* **42** 3936 (1990)
20. Bartolo N, Matarrese S, Riotto A *JHEP* (04) 006 (2004); astro-ph/0308088
21. Bartolo N et al. *Phys. Rep.* **402** 103 (2004); astro-ph/0406398
22. Komatsu E et al. *Astrophys. J. Suppl.* **180** 330 (2009); arXiv:0803.0547
23. Gümrükcüoğlu A E, Contaldi C R, Peloso M, in *On Recent Developments in Theoretical and Experimental General Relativity, Gravitation and Relativistic Field Theories. Proc. of the 11th Marcel Grossmann Meeting on General Relativity, 23 – 29 July 2006, Berlin, Germany* (Eds H Kleinert, R T Jantzen) (Singapore: World Scientific, 2008) p. 1641; astro-ph/0608405
24. Gümrükcüoğlu A E, Contaldi C R, Peloso M *JCAP* (11) 005 (2007); arXiv:0707.4179
25. Ackerman L, Carroll S M, Wise M B *Phys. Rev. D* **75** 083502 (2007); "Erratum" *Phys. Rev. D* **80** 069901(E) (2009); astro-ph/0701357
26. Watanabe M, Kanno S, Soda J *Phys. Rev. Lett.* **102** 191302 (2009); arXiv:0902.2833
27. Dimopoulos K, Karčiauskas M, Wagstaff J M *Phys. Rev. D* **81** 023522 (2010); arXiv:0907.1838
28. Watanabe M, Kanno S, Soda J *Prog. Theor. Phys.* **123** 1041 (2010)
29. Dulaney T R, Gresham M I *Phys. Rev. D* **81** 103532 (2010); arXiv:1001.2301
30. Gümrükcüoğlu A E, Himmetoglu B, Peloso M *Phys. Rev. D* **81** 063528 (2010); arXiv:1001.4088
31. Starobinsky A A *Pis'ma Zh. Eksp. Teor. Fiz.* **57** 606 (1993) [*JETP Lett.* **57** 622 (1993)]; gr-qc/9305019
32. de Oliveira-Costa A, Smoot G F, Starobinsky A A *Astrophys. J.* **468** 457 (1996); astro-ph/9705125
33. Inoue K T, Tomita K, Sugiyama N *Mon. Not. R. Astron. Soc.* **314** L21 (2000); astro-ph/9906304
34. Dineen P, Rocha G, Coles P *Mon. Not. R. Astron. Soc.* **358** 1285 (2005); astro-ph/0404356
35. Kunz M et al. *Phys. Rev. D* **77** 023525 (2008)
36. Turok N *Phys. Scripta* **T36** 135 (1991)
37. Turok N, Spergel D *Phys. Rev. Lett.* **64** 2736 (1990)
38. Durrer R *New Astron. Rev.* **43** 111 (1999)
39. Cruz M et al. *Science* **318** 1612 (2007); arXiv:0710.5737
40. Jaffe T R et al. *Astrophys. J.* **629** L1 (2005); astro-ph/0503213
41. Demiański M, Doroshkevich A G *Phys. Rev. D* **75** 123517 (2007)
42. Durrer R, Kahniashvili T, Yates A *Phys. Rev. D* **58** 123004 (1998); astro-ph/9807089

[5] http://www.glesp.nbi.dk

43. Mack A, Kahniashvili T, Kosowsky A *Phys. Rev. D* **65** 123004 (2002); astro-ph/0105504
44. Naselsky P D, Chiang L-Y, Olesen P, Verkhodanov O V *Astrophys. J.* **615** 45 (2004); astro-ph/0405181
45. Kahniashvili T, Ratra B *Phys. Rev. D* **71** 103006 (2005); astro-ph/0503709
46. Kahniashvili T, Lavrelashvili G, Ratra B *Phys. Rev. D* **78** 063012 (2008); arXiv:0807.4239
47. Tauber J A et al. *Astron. Astrophys.* **520** A1 (2010)
48. Naselsky P D, Novikov D I, Novikov I D *The Physics of the Cosmic Microwave Background* (Cambridge: Cambridge Univ. Press, 2006)
49. Gorbunov D S, Rubakov V A *Vvedenie v Teoriyu Rannei Vselennoi: Kosmologicheskie Vozmushcheniya. Inflyatsionnaya Teoriya* (Introduction to the Theory of the Early Universe: Cosmological Perturbations and Inflationary Theory) (Moscow: KRASAND, 2010) [Translated into English (Singapore: World Scientific, 2011)]
50. Lukash V N, Mikheeva E V *Fizicheskaya Kosmologiya* (Physical Cosmology) (Moscow: Fizmatlit, 2010)
51. Kim J, Naselsky P *Phys. Rev. D* **79** 123006 (2009)
52. Yadav A P S, Wandelt B D *Adv. Astron.* **2010** 565248 (2010); arXiv:1006.0275
53. Bartolo N, Matarrese S, Riotto A *Adv. Astron.* **2010** 157079 (2010); arXiv:1001.3957
54. Komatsu E et al., Astro2010: The Astronomy and Astrophysics Decadal Survey. Science White Papers, No. 59; arXiv:0902.4759
55. Komatsu E *Class. Quantum Grav.* **27** 124010 (2010)
56. Libanov M, Ramazanov S, Rubakov V *JCAP* (06) 010 (2011); arXiv:1102.1390
57. Libanov M, Mironov S, Rubakov V *Phys. Rev. D* **84** 083502 (2011); arXiv:1105.6230
58. Creminelli P et al. *JCAP* (02) 006 (2011); arXiv:1011.3004
59. Verde L et al. *Mon. Not. R. Astron. Soc.* **313** 141 (2000)
60. Lesgourgues J et al. *Phys. Rev. D* **71** 103514 (2005); astro-ph/0412551
61. Lewis A, Challinor A, Hanson D *JCAP* (03) 018 (2011); arXiv:1101.2234
62. Semenova T A, Pariiskii Yu N, Bursov N N *Astron. Rep.* **53** 1 (2009)
63. Komatsu E, Spergel D N *Phys. Rev. D* **63** 063002 (2001); astro-ph/0005036
64. Seljak U, Zaldarriaga M *Astrophys. J.* **469** 437 (1996)
65. Lyth D H, Wands D *Phys. Lett. B* **524** 5 (2002); hep-ph/0110002
66. Moroi T, Takahashi T *Phys. Lett. B* **522** 215 (2001); ''Erratum'' *Phys. Lett. B* **539** 303 (2002); hep-ph/0110096
67. Creminelli P et al. *JCAP* (05) 004 (2006); astro-ph/0509029
68. Senatore L, Smith K M, Zaldarriaga M *JCAP* (01) 028 (2010); arXiv:0905.3746
69. Bennett C L et al. *Astrophys. J. Suppl.* **192** 17 (2011); arXiv:1001.4758
70. Komatsu E et al. *Astrophys. J. Suppl.* **148** 119 (2003); astro-ph/0302223
71. Spergel D N et al. *Astrophys. J. Suppl.* **170** 377 (2007); astro-ph/0603449
72. Komatsu E et al. *Astrophys. J. Suppl.* **192** 18 (2011); arXiv:1001.4538
73. Slosar A et al. *JCAP* (08) 031 (2008)
74. Bennett C L et al. *Astrophys. J. Suppl.* **148** 1 (2003); astro-ph/0302207
75. Bennett C L et al. *Astrophys. J. Suppl.* **148** 97 (2003); astro-ph/0302208
76. Spergel D N et al. *Astrophys. J. Suppl.* **148** 175 (2003); astro-ph/0302209
77. Hinshaw G et al. *Astrophys. J. Suppl.* **170** 288 (2007); astro-ph/0603451
78. Hinshaw G et al. *Astrophys. J. Suppl.* **180** 225 (2009); arXiv:0803.0732
79. Jarosik N et al. *Astrophys. J. Suppl.* **192** 14 (2011); arXiv:1001.4744
80. Chiang L-Y, Naselsky P D, Verkhodanov O V, Way M J *Astrophys. J.* **590** L65 (2003); astro-ph/0303643
81. Naselsky P D, Doroshkevich A G, Verkhodanov O V *Astrophys. J.* **599** L53 (2003); astro-ph/0310542
82. Coles P et al. *Mon. Not. R. Astron. Soc.* **350** 989 (2004)
83. Vielva P et al. *Astrophys. J.* **609** 22 (2004); astro-ph/0310273
84. Park C-G *Mon. Not. R. Astron. Soc.* **349** 313 (2004)
85. Eriksen H K et al. *Astrophys. J.* **612** 64 (2004); astro-ph/0401276
86. Eriksen H K et al. *Astrophys. J.* **605** 14 (2004)
87. Hansen F K et al. *Astrophys. J.* **607** L67 (2004)
88. Larson D L, Wandelt B D *Astrophys. J.* **613** L85 (2004)
89. Schwarz D J et al. *Phys. Rev. Lett.* **93** 221301 (2004)
90. de Oliveira-Costa A et al. *Phys. Rev. D* **69** 063516 (2004)
91. Land K, Magueijo J *Phys. Rev. Lett.* **95** 071301 (2005)
92. Cruz M et al. *Mon. Not. R. Astron. Soc.* **369** 57 (2006)
93. Naselsky P D, Verkhodanov O V, Nielsen M T B *Astrofiz. Byull.* **63** 231 (2007) [*Astrophys. Bull.* **63** 216 (2007)]; arXiv:0707.1484
94. Copi C J et al. *Phys. Rev. D* **75** 023507 (2007)
95. Rakić A, Schwarz D J *Phys. Rev. D* **75** 103002 (2007)
96. Hoftuft J et al. *Astrophys. J.* **699** 985 (2009); arXiv:0903.1229
97. Kim J, Naselsky P *Astrophys. J.* **714** L265 (2010)
98. Hansen M et al. *Phys. Rev. D* **83** 103508 (2011); arXiv:1103.6135
99. Gold B et al. *Astrophys. J. Suppl.* **192** 15 (2011); arXiv:1001.4555
100. Leach S M et al. *Astron. Astrophys.* **491** 597 (2008); arXiv:0805.0269
101. Doroshkevich A, Verkhodanov O *Phys. Rev. D* **83** 043002 (2011); arxiv:1008.4094
102. Kim J, Naselsky P, Christensen P R *Phys. Rev. D* **79** 023003 (2009)
103. Stolyarov V et al. *Mon. Not. R. Astron. Soc.* **336** 97 (2002)
104. Tegmark M, de Oliveira-Costa A, Hamilton A J S *Phys. Rev. D* **68** 123523 (2003)
105. Reichardt C L et al. *Astrophys. J.* **694** 1200 (2009)
106. Brown M L et al. *Astrophys. J.* **705** 978 (2009)
107. Bardeen J M et al. *Astrophys. J.* **304** 15 (1986)
108. Bond J R, Efstathiou G *Mon. Not. R. Astron. Soc.* **226** 655 (1987)
109. Watts P, Coles P *Mon. Not. R. Astron. Soc.* **338** 806 (2003)
110. Coles P, Chiang L-Y *Nature* **406** 376 (2000)
111. Chiang L-Y, Naselsky P D, Coles P *Astrophys. J.* **602** L1 (2004); astro-ph/0208235
112. Naselsky P D, Doroshkevich A G, Verkhodanov O V *Mon. Not. R. Astron. Soc.* **349** 695 (2004); astro-ph/0310601
113. Fisher N I *Statistical Analysis of Circular Data* (Cambridge: Cambridge Univ. Press, 1993)
114. Khabibullina M L, Verkhodanov O V, Parijskij Yu N *Astrofiz. Byull.* **63** 101 (2008) [*Astrophys. Bull.* **63** 95 (2008)]
115. Naselsky P D, Verkhodanov O V *Astrofiz. Byull.* **62** 218 (2007) [*Astrophys. Bull.* **62** 203 (2007)]
116. Naselsky P D, Verkhodanov O V *Int. J. Mod. Phys. D* **17** 179 (2008); astro-ph/0609409
117. Chiang L-Y et al. *JCAP* (01) 021 (2007); astro-ph/0608421
118. Verkhodanov O V, Khabibullina M L, Majorova E K *Astrofiz. Byull.* **64** 272 (2009) [*Astrophys. Bull.* **64** 263 (2009)]; arXiv:0912.3073
119. Verkhodanov O V, Khabibullina M L *Astrofiz. Byull.* **65** 413 (2010) [*Astrophys. Bull.* **65** 390 (2010)]
120. Verkhodanov O V et al. *Astrofiz. Byull.* **65** 252 (2010) [*Astrophys. Bull.* **65** 238 (2010)]; arXiv: 1009.3720
121. Naiden Ya V, Verkhodanov O V *Astrofiz. Byull.* **66** 372 (2011) [*Astrophys. Bull.* **66** 345 (2011)]
122. Copi C J, Huterer D, Starkman G D *Phys. Rev. D* **70** 043515 (2004); astro-ph/0310511
123. Copi C J et al. *Mon. Not. R. Astron. Soc.* **367** 79 (2006); astro-ph/0508047
124. Maxwell J C *A Treatise on Electricity and Magnetism* Vol. 1, 3rd ed. (Oxford: Clarendon Press, 1892)
125. Pullen A R, Kamionkowski M *Phys. Rev. D* **76** 103529 (2007); arXiv:0709.1144
126. Hanson D, Lewis A *Phys. Rev. D* **80** 063004 (2009); arXiv:0908.0963
127. Groeneboom N E, Eriksen H K *Astrophys. J.* **690** 1807 (2009); arXiv:0807.2242
128. Groeneboom N E et al. *Astrophys. J.* **722** 452 (2010); arXiv:0911.0150
129. Minkowski H *Math. Ann.* **57** 447 (1903)
130. Mecke K R, Buchert T, Wagner H *Astron. Astrophys.* **288** 697 (1994)
131. Schmalzing J, Buchert T *Astrophys. J.* **482** L1 (1997)
132. Doroshkevich A G *Astrofiz.* **6** 581 (1970) [*Astrophysics* **6** 320 (1970)]
133. Gott J R (III) et al. *Astrophys. J.* **352** 1 (1990)
134. Naselsky P D, Novikov D I *Astrophys. J.* **444** L1 (1995)
135. Novikov D, Schmalzing J, Mukhanov V F *Astron. Astrophys.* **364** 17 (2000); astro-ph/0006097
136. Novikov D I et al. *Int. J. Mod. Phys. D* **10** 245 (2001)

137. Schmalzing J, Gorski K M *Mon. Not. R. Astron. Soc.* **297** 355 (1998)
138. Winitzki S, Kosowsky A *New Astron.* **3** 75 (1998)
139. Novikov D, Colombi S, Doré O *Mon. Not. R. Astron. Soc.* **366** 1201 (2006); astro-ph/0307003
140. Hikage C et al. *Mon. Not. R. Astron. Soc.* **389** 1439 (2008); arXiv:0802.3677
141. Yadav A P S, Wandelt B D *Phys. Rev. Lett.* **100** 181301 (2008)
142. Cruz M et al. *Mon. Not. R. Astron. Soc.* **356** 29 (2005)
143. Pando J, Valls-Gabaud D, Fang L-Z *Phys. Rev. Lett.* **81** 4568 (1998)
144. Barreiro R B et al. *Mon. Not. R. Astron. Soc.* **318** 475 (2000)
145. Cayón L et al. *Mon. Not. R. Astron. Soc.* **326** 1243 (2001)
146. Martínez-González E et al. *Mon. Not. R. Astron. Soc.* **336** 22 (2002); astro-ph/0111284
147. Cayón L et al. *Mon. Not. R. Astron. Soc.* **339** 1189 (2003)
148. Antoine J-P, Vandergheynst P *J. Math. Phys.* **39** 3987 (1998)
149. Haslam C G T et al. *Astron. Astrophys. Suppl.* **47** 1 (1982)
150. Zhang R, Huterer D *Astropart. Phys.* **33** 69 (2010); arXiv:0908.3988
151. Rudnick L, Brown S, Williams L R *Astrophys. J.* **671** 40 (2007); arXiv:0704.0908
152. Condon J J et al. *Astron. J.* **115** 1693 (1998)
153. Smith K M, Huterer D *Mon. Not. R. Astron. Soc.* **403** 2 (2010); arXiv:0805.2751
154. Naselsky P D et al. *Astrofiz. Byull.* **65** 107 (2010) [*Astrophys. Bull.* **65** 101 (2010)]; arXiv:0712.1118
155. Verkhodanov O V et al. *Astrofiz. Byull.* **63** 389 (2008) [*Astrophys. Bull.* **63** 366 (2008)]; arXiv:0902.0281
156. Smith K M, Huterer D *Mon. Not. R. Astron. Soc.* **403** 2 (2010); arXiv:0805.2751
157. Solov'ev D I, Verkhodanov O V *Astrofiz. Byull.* **65** 128 (2010) [*Astrophys. Bull.* **65** 121 (2010)]
158. Verkhodanov O V, Basova A A *Astrofiz. Byull.* **66** 436 (2011) [*Astrophys. Bull.* **66** 407 (2011)]
159. Narcowich F J, Petrushev P, Ward J D *SIAM J. Math. Analysis* **38** 574 (2006)
160. Narcowich F, Petrushev P, Ward J *J. Funct. Anal.* **238** 530 (2006)
161. Rudjord Ø et al. *Astrophys. J.* **701** 369 (2009); arXiv:0901.3154
162. Marinucci D et al. *Mon. Not. R. Astron. Soc.* **383** 539 (2008)
163. Doroshkevich A G et al. *Int. J. Mod. Phys. D* **14** 275 (2005); astro-ph/0305537
164. Doroshkevich A G et al. *Int. J. Mod. Phys. D* **20** 1053 (2011); arXiv: 0904.2517